

# Targeting the UFL1-AKT Cascade Suppresses Triple-Negative Breast Cancer Progression

Corresponding Author: Professor Tongzheng Liu

**This file contains all reviewer reports in order by version, followed by all author rebuttals in order by version.**

Version 0:

Reviewer comments:

Reviewer #1

(Remarks to the Author)

Summary: In this manuscript, Xiao Yang et al identified and characterized a previously unrecognized oncogenic feedback loop between UFL1-mediated UFMylation and AKT phosphorylation in triple-negative breast cancer (TNBC). They demonstrate that UFL1 directly interacts with AKT1, catalyzing its UFMylation at Lys189, Lys276, and Lys297, which significantly enhances AKT1 phosphorylation and activity. Reciprocally, AKT1 phosphorylates UFL1 at Thr426, further enhancing UFMylation activity. In addition, genetic depletion of UFL1 remarkably inhibited cell proliferation and enhanced sensitivity to chemotherapies in mouse xenograft models. Disrupting the AKT1-UFL1 interaction using a cell-penetrating peptide (PDAU-TAT) suppresses tumor growth in both cell line- and patient-derived xenograft models. The study provides mechanistic insight into AKT1 hyperactivation in TNBC and proposes a novel therapeutic axis for intervention.

Overall assessment: This work presents a novel and conceptually strong advance with implications for understanding post-translational regulation of AKT signaling. The identification of UFMylation as a critical regulatory layer and the development of a peptide-based disruption strategy are both innovative and translationally relevant. The mechanistic and functional data are extensive and largely convincing. However, several key points need to be addressed to fully support the proposed model and ensure broad relevance.

Major Points:

- + Context specificity of the UFL1-AKT axis in TNBC: While the study focuses on TNBC, data in ER+ and HER2+ breast cancer models (Supplementary Fig. 1) suggest that UFL1-mediated AKT regulation may not be exclusive to TNBC. Please clarify whether this mechanism is specific to TNBC or generalizable across subtypes. Quantitative comparisons and discussion of subtype-specific dependency would strengthen the narrative.
- + Biochemical evidence for AKT1 UFMylation in AKT activation: A key mechanistic claim of the manuscript is that UFMylation of AKT1 at K189, K276, and K297 is required for its phosphorylation at T308 and S473. However, in standard cellular models (including our own lab's experience and widely published studies), insulin or IGF-1 stimulation induces robust AKT1 phosphorylation without any observable upward shift in AKT1 molecular weight on Western blot with the phospho-AKT1 specific antibodies. This raises an important question: if UFMylation were required for AKT activation, why is the fully activated AKT with both p-T308 and p-S473 readily observed in the absence of a UFM1-dependent band shift in these common settings? Please clarify whether the proposed UFL1-AKT1 UFMylation axis is before AKT activation and whether the de-UFMylation of fully activated AKT1 happened?
- + UFMylation of AKT1 in TNBC context: The identification of AKT1 Lysines 189, 276 and 297 ufmylated by UFL1 is quite promising, however, Figure 2 i, j, k have been used human kidney cell line HEK293 is not appropriate in the claimed scope of TNBC, the authors must perform these experiments with TNBC cell lines such as MDA-MB-231 and HCC1806 as used in other experiments (Fig 1).
- + Mechanistic insight for UFL1 T426 phosphorylation: The data support AKT1-mediated phosphorylation of UFL1 at T426, but the downstream effect, i.e., how this modification structurally or functionally enhances UFL1's enzymatic activity—is still unclear with only connection with AKT1 phosphorylations and AKT downstream. The authors should provide additional biochemical or structural rationale, if available, or acknowledge this limitation and discuss potential mechanisms.
- + Therapeutic characterization of PDAU-TAT: The PDAU-TAT peptide shows promising anti-tumor effects, but key pharmacological parameters (e.g., half-life, in vivo stability, biodistribution, immune tolerance) are not described or addressed. Please provide further data (if available) or discuss the limitations and future work needed to validate PDAU as a therapeutic agent.
- + Quantification of IHC data: The IHC analysis linking pUFL1 and pAKT in Figure 6 is promising, but the scoring approach

and representative images require further clarification. Please include a more detailed description of scoring methods and representative high-quality images in the supplementary data, and clarify how the correlation and regression line were generated. If outliers influence the result, a residual plot or alternative correlation analysis would be helpful for clarity.

Minor points:

- + The Discussion is quite dense, please consider focusing more sharply on the most novel aspects. Figure legends should more consistently cross-reference supplementary figures and provide necessary experimental context (e.g., replicate numbers, statistical tests).
- + Please revise the manuscript for typo errors and awkward phrasing, particularly in the Methods section.

Reviewer #2

(Remarks to the Author)

The manuscript "Targeting the UFL1-AKT Cascade Suppresses Triple Negative Breast Cancer Progression" by Yang, Wen and Ma et al., describes a new interesting positive feedback loop between AKT1 UFMylation and UFL1 phosphorylation. Following the identification of this link, the authors create a cell-penetrant peptide that blocks the interaction and leads to in vivo anti-tumour efficacy.

Overall, the manuscript is well written and has a logical structure. I only have a few comments.

Major comments:

- If any conclusions are to be made from the IF experiment in Supp Fig 1e they should be repeated at much higher magnification, and co-localizations should be quantified.
- Along the same line. I understand that many of the IP experiments are hard to quantify, but the authors should provide quantification and statistics for all claims based on regular western blotting experiments (Fx Fig 1k and l, but many more).

Minor comments:

- Figure 1i: I think MDA-MB-231 are missing in the figure?
- Line 168: UFMylation of AKT1 was detected by a 20kDa shift compared to unmodified AKT1. This seems rather unspecific. Is it not possible to validate with alternate methods? Fx m/s?
- Should the correlation plot in Fig. 6c not have 40 dots?

Reviewer #3

(Remarks to the Author)

The manuscript by Yang et al reports a novel finding of a positive feed-back loop between UFM1 E3 ligase UFL1 and AKT1 in triple negative breast cancer (TNBC) cells. The authors have demonstrated that UFL1-mediated UFMylation enhances AKT1 phosphorylation and activation, thereby promoting tumor progression and drug resistance. Disruption of the UFL1-AKT1 interaction by a specific peptide significantly inhibits tumor progression, suggesting that the UFL-AKT1 axis may serve as a novel therapeutic target for TNBC treatment. The study uncovers a novel relationship between UFMylation and AKT1 and expands current understanding of the role of UFMylation in tumor progression. Most experiments were well-designed and executed, and the conclusions were generally supported by the data. However, more mechanistic studies are needed to support the proposed working model. Further investigation of this novel interaction in UFMylation biology would broaden the scope of the current study.

Specific comments:

1. In Fig.1m and n, a group of 'vector+Capivaserib" should be included. The effect of Capivaserib on phosphorylation of AKT substrates should be examined as in Fig.1i.
2. In Fig. 2a, does Flag antibody detect UFMylated AKT1? Similarly, does AKT antibody detect UFMylated form of endogenous AKT in Fig.2c? In Fig. 2, some UFMylated AKT1 were around 100 kD, while others were well below 100 kD marker. Please be consistent. Also please specify the cell line used in Fig. 2e, 2g, 2j and 2k.
3. Fig. 3. It may be more appropriate to move Fig.2j and k to Fig. 3. Although AKT1 3KR mutant altered its interactions with the components of mTORC2 and PP2A complexes, it was not definitive evidence supporting the conclusion as claimed in the manuscript. It does not rule out the possibility that the mutation itself may affect the interaction. Therefore, more biochemical data may be needed to support the conclusion that happens to be the major point of the proposed working model. The authors should test the interaction between AKT and its regulators in UFM1 or UFL1 depleted cells. Moreover, the authors should compare the interactions between UFMylated and unmodified AKT1 with its regulators in a more direct assay.
4. Fig. 4. The finding of UFL1 phosphorylation by AKT is quite intriguing. It would be interesting to investigate the effect of this phosphorylation on overall UFMylation and other UFM1 targets such as RPL26 and ER $\alpha$ .
5. Fig.5. The effect of PDAU on UFL1 phosphorylation and overall UFMylation should be examined.
6. Fig.6. The observation of the correlation between pUFL1 and pAKT in TNBCs is interesting, but its clinical relevance is unclear. As suggested above, more experimental data are needed to back up the working model. Since AKT is the ultimate executioner to promote tumor progression in this model, what is the advantage of PDAU comparing to AKT inhibitors?

#### Reviewer #4

##### (Remarks to the Author)

In this manuscript, Liu and colleagues reported a positive feedback loop between UFL1 and AKT through UFL1-mediated UFMylation of AKT1 and AKT-mediated phosphorylation. The loop results in a sustained activation of both pro-oncogenic regulators, the disruption of which inhibits TNBC progression. They also demonstrate that high level of UFL1 phosphorylation is associated with increased AKT phosphorylation in clinical samples. Overall, the work provides new insights into drug resistance of TNBC. However, more evidence is required before the publication. Detailed comments are listed below.

1. The authors have successfully proved that UFL1 has direct interaction with AKT1. They also generate mutants to map the sites that may influence UFMylation of AKT1. The authors may consider to identify UFMylated peptide fragments of AKT1 using mass spectrometry.
2. In addition, the authors showed that K189, K276 and K297 are sites of UFMylation. A discussion on the influence of UFMylation on protein conformation, binding or further modification should be discussed. Since the molecular structure of human AKT1 has been published, a structure-based discussion may be helpful.
3. In Figure 3f, a semi-quantification of the levels of Ki67 and cleaved PARP1 should be performed.
4. The authors found that Thr426 was phosphorylated by AKT1. Mass spectrometry should be used to confirm this finding and to explore whether there is additional site of phosphorylation.
5. Peptide derived from UFL1 20-30 was developed as an antagonist that disrupt interaction between UFL1 and AKT. The K<sub>d</sub> of PDAU should be determined to quantify the affinity of the resulting peptide to AKT, using WT UFL1 and NP as controls. In addition, the distribution of PDAU in the tumors and other organs should be quantified.
6. The efficacy and safety of PDAU and AKT inhibitor capivasertib should be compared directly to demonstrate the potential application of modulating the discovered protein-protein interaction.

Version 1:

Reviewer comments:

#### Reviewer #1

##### (Remarks to the Author)

This revised manuscript provides new data supporting a model in which UFL1-mediated UFMylation of AKT1 enhances its activation and downstream signaling in triple-negative breast cancer (TNBC). The authors have substantially improved the manuscript by expanding validation across multiple cell lines, clarifying mechanistic steps, and including new time-course and UFSP2-knockdown experiments to address the transient nature of AKT1 UFMylation. The additional data supporting the transient and low-stoichiometry nature of AKT1 UFMylation, as well as the explanation of UFSP2's regulatory role, make the mechanistic model much clearer. The figures and legends are also improved and well presented.

#### Reviewer #2

##### (Remarks to the Author)

My concerns have been addressed. I have no further concerns.

#### Reviewer #3

##### (Remarks to the Author)

The authors have satisfactorily addressed the comments of this reviewer

#### Reviewer #4

##### (Remarks to the Author)

In the revised manuscript, the authors have performed protein modeling and ITC to elucidate the possible mechanism, and have explored the biodistribution, efficacy and safety of the PDAU and capivasertib to evaluate the therapeutic potential of the drugs. Although the authors failed to provide MS data that were requested by the reviewer, they have provided more biochemical evidence and reasonable explanation to support their major claims. Overall, the authors present a significant finding that is crucial for TNBC, the main claims of which are supported by the data in the revised manuscript. I have no further question.

**Open Access** This Peer Review File is licensed under a Creative Commons Attribution 4.0 International License, which permits use, sharing, adaptation, distribution and reproduction in any medium or format, as long as you give appropriate credit to the original author(s) and the source, provide a link to the Creative Commons license, and indicate if changes were made.

In cases where reviewers are anonymous, credit should be given to 'Anonymous Referee' and the source.

The images or other third party material in this Peer Review File are included in the article's Creative Commons license, unless indicated otherwise in a credit line to the material. If material is not included in the article's Creative Commons license and your intended use is not permitted by statutory regulation or exceeds the permitted use, you will need to obtain permission directly from the copyright holder.

To view a copy of this license, visit <https://creativecommons.org/licenses/by/4.0/>

Reviewer #1 (AKT activation and posttranslational modifications, Remarks to the Author):

Summary: In this manuscript, Xiao Yang et al identified and characterized a previously unrecognized oncogenic feedback loop between UFL1-mediated UFMylation and AKT phosphorylation in triple-negative breast cancer (TNBC). They demonstrate that UFL1 directly interacts with AKT1, catalyzing its UFMylation at Lys189, Lys276, and Lys297, which significantly enhances AKT1 phosphorylation and activity. Reciprocally, AKT1 phosphorylates UFL1 at Thr426, further enhancing UFMylation activity. In addition, genetic depletion of UFL1 remarkably inhibited cell proliferation and enhanced sensitivity to chemotherapies in mouse xenograft models. Disrupting the AKT1-UFL1 interaction using a cell-penetrating peptide (PDAU-TAT) suppresses tumor growth in both cell line- and patient-derived xenograft models. The study provides mechanistic insight into AKT1 hyperactivation in TNBC and proposes a novel therapeutic axis for intervention.

Overall assessment: This work presents a novel and conceptually strong advance with implications for understanding post-translational regulation of AKT signaling. The identification of UFMylation as a critical regulatory layer and the development of a peptide-based disruption strategy are both innovative and translationally relevant. The mechanistic and functional data are extensive and largely convincing. However, several key points need to be addressed to fully support the proposed model and ensure broad relevance.

---

Major Points:

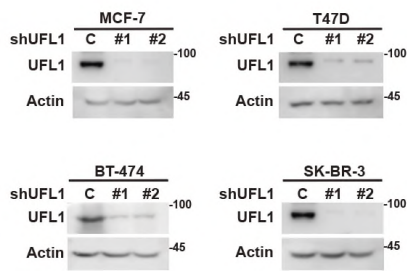
+ Context specificity of the UFL1-AKT axis in TNBC: While the study focuses on TNBC, data in ER+ and HER2+ breast cancer models (Supplementary Fig. 1) suggest that UFL1-mediated AKT regulation may not be exclusive to TNBC. Please clarify whether this mechanism is specific to TNBC or generalizable across subtypes. Quantitative comparisons and discussion of subtype-specific dependency would strengthen the narrative.

We sincerely thank the reviewer for this insightful comment. Our data demonstrate that the UFL1-AKT axis is not restricted to TNBC subtype but is conserved across ER<sup>+</sup>, HER2<sup>+</sup>, and TNBC breast cancer models. To address this point, we have now provided additional quantitative comparisons.

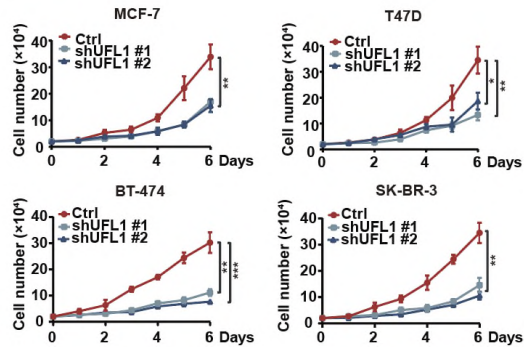
As shown in Supplementary Fig. 1a-d, UFL1 depletion inhibited proliferation and enhanced chemosensitivity not only in TNBC but also in ER<sup>+</sup> (MCF-7 and T47D) and HER2<sup>+</sup> (BT-474 and SK-BR-3) cell lines. Quantitative analyses showed that the magnitude of growth inhibition upon UFL1 knockdown was comparable across different breast cancer subtypes. Consistently, UFL1 knockdown or overexpression in ER<sup>+</sup>(MCF-7 and T47D) and HER2<sup>+</sup> models (BT-474 and SK-BR-3) altered phosphorylation of AKT and its downstream target GSK3 $\beta$  and PRAS40 similarly to in TNBC (Supplementary Fig. 1g, h). Moreover, UFL1 promotes AKT UFMylation in ER<sup>+</sup> and HER2<sup>+</sup> cells (Supplementary Fig. 2d-g), indicating that AKT1 UFMylation is a conserved mechanism across breast cancer subtypes.

In line with the reviewer's comment, we have revised the Discussion accordingly to emphasize this broader relevance and to highlight the therapeutic potential of targeting the UFL1-AKT axis across diverse breast cancer contexts.

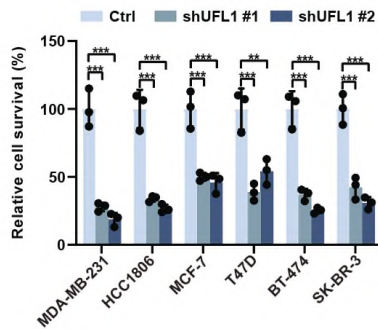
Supplementary Fig. 1a



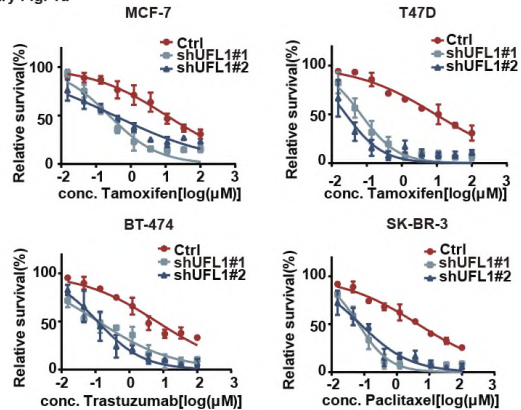
Supplementary Fig. 1b



Supplementary Fig. 1c

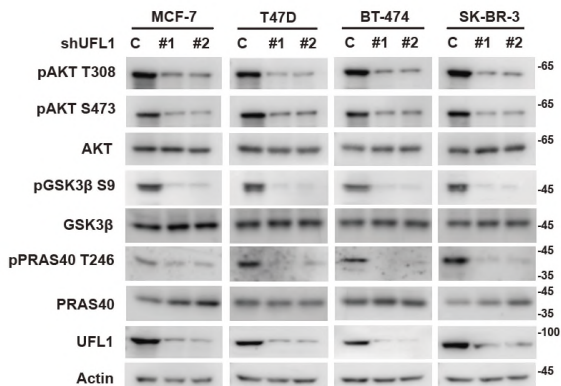


Supplementary Fig. 1d

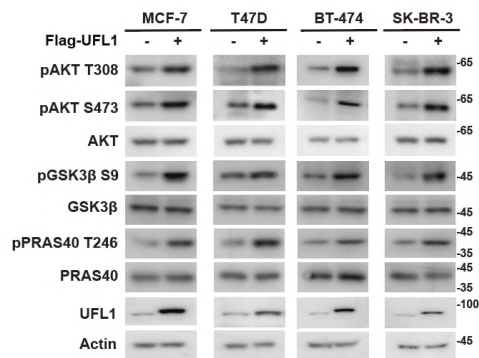


a, MCF-7, T47D, BT-474 and SK-BR-3 cells stably expressing control or UFL1 shRNAs were generated, and western blotting was performed using the indicated antibodies. b, Cell proliferation as in (a) was measured, and results represent the mean  $\pm$  SD of three independent experiments. c, Relative cell survival in various breast cancer cell lines (MDA-MB-231, HCC1806, MCF-7, T47D, BT-474, SK-BR-3) upon depletion of UFL1. d, MCF-7, T47D, BT-474 and SK-BR-3 cells stably expressing control or UFL1 shRNAs were treated with the indicated concentrations of tamoxifen, trastuzumab or paclitaxel and cell survival was determined. Results represent the mean  $\pm$  SD of three independent experiments. Data showed as the mean  $\pm$  SD were analyzed by one-way ANOVA. \* $p < 0.05$ , \*\* $p < 0.01$ , \*\*\* $p < 0.001$ .

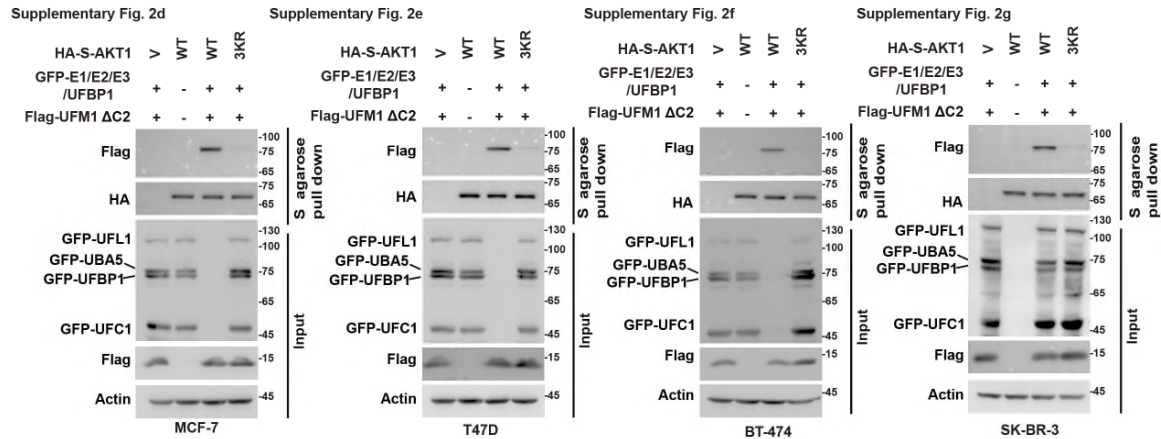
Supplementary Fig. 1g



Supplementary Fig. 1h



**g**, MCF-7, T47D, BT-474 and SK-BR-3 cells stably expressing control or UFL1 shRNAs were generated, and western blotting was performed using the indicated antibodies. **h**, MCF-7, T47D, BT-474 and SK-BR-3 cells were transfected with empty vector or Flag-UFL1. Western blot was performed with indicated antibodies.



**d-g**, UFMylation assay of the HA-S-AKT1 WT and 3KR was performed in MCF-7 (d), T47D (e), BT-474 (f) and SK-BR-3 (g) cells expressing the indicated components of the UFMylation system.

+ Biochemical evidence for AKT1 UFMylation in AKT activation: A key mechanistic claim of the manuscript is that UFMylation of AKT1 at K189, K276, and K297 is required for its phosphorylation at T308 and S473. However, in standard cellular models (including our own lab's experience and widely published studies), insulin or IGF-1 stimulation induces robust AKT1 phosphorylation without any observable upward shift in AKT1 molecular weight on Western blot with the phospho-AKT1 specific antibodies. This raises an important question: if UFMylation were required for AKT activation, why is the fully activated AKT with both p-T308 and p-S473 readily observed in the absence of a UFM1-dependent band shift in these common settings? Please clarify whether the proposed UFL1-AKT1 UFMylation axis is before AKT activation and whether the de-UFMylation of fully activated AKT1 happened?

We thank the reviewer for this critical comment, which allows us to clarify the dynamic and transient nature of AKT1 UFMylation during activation.

First, it is important to note that AKT1 undergoes several post-translational modifications that are not consistently detected by mobility shifts on western blot. For instance, Skp2-mediated K63-linked polyubiquitination at K8/K14 and SUMOylation at K276 of AKT1 have been shown to regulate AKT1 activation, yet these modifications do not cause detectable electrophoretic mobility shifts when probed with phosphor-AKT antibody in previous manuscripts<sup>1, 2</sup>. This reflects the highly dynamic and reversible nature of these post-translational modifications, such as SUMOylation, which could be removed by SENP family proteases<sup>2, 3</sup>. By analogy, we propose that UFMylation of AKT1 is similarly transient and therefore not readily captured by standard phosphor-AKT antibody in western blotting process.

To address the temporal relationship, we performed insulin stimulation time-course experiments and observed that AKT1 UFMylation peaked at 15 min upon insulin treatment, preceding maximal Ser473 phosphorylation

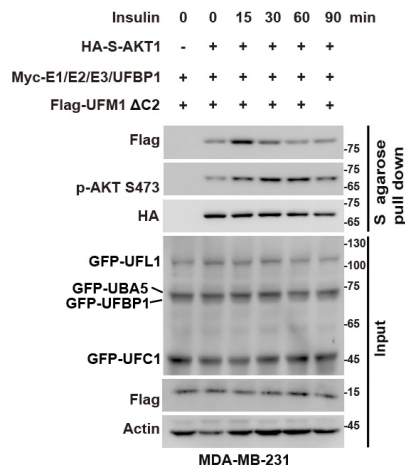
(Supplementary Fig. 3a). This supports the notion that UFMylation may function as an upstream priming event for AKT activation.

We then investigated the role of de-UFMylation in AKT activation. Depletion of the UFM1-specific protease UFSP2 led to a marked accumulation of UFMylated AKT1 in both control and UFMylation machinery components-transfected MDA-MB-231 cells (Supplementary Fig. 3m). Moreover, UFSP2 showed preferential binding to activated AKT1 mutant (T308D, S473D or T308D/S473D) compared to inactive AKT1 mutant (T308A, S473A or T308A/S473A)<sup>4</sup> (Supplementary Fig. 3r), suggesting that once AKT1 is phosphorylated, UFSP2 rapidly interacts and removes UFMylation. The de-UFMylation process may be important for AKT's accessibility to downstream substrates, since sites of UFMylation Lys189, Lys276, and Lys297 are located within the catalytic domain and could otherwise create steric hindrance. Supporting this model, overexpression of UFL1 under UFSP2 knockdown conditions produced a shifted band of phosphorylation AKT co-migrating with UFMylated AKT1 (Supplementary Fig. 3p). Furthermore, immunoprecipitation with anti-p-AKT S473 antibody revealed detectable UFMylated AKT only when UFSP2 was depleted (Supplementary Fig. 3q).

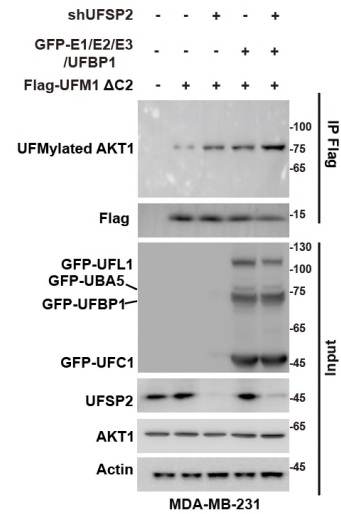
Taken together, these findings indicate that AKT1 UFMylation is a transient but essential priming step for AKT activation. Rapid UFSP2-mediated de-UFMylation following phosphorylation explains the absence of a stable UFMylated-AKT band in conventional western blotting assays. This dynamic cycle parallels the regulatory logic of other reversible post-translational modifications and underscores the importance of perturbing the UFM1 pathway such as by UFSP2 depletion to reveal this regulatory layer.



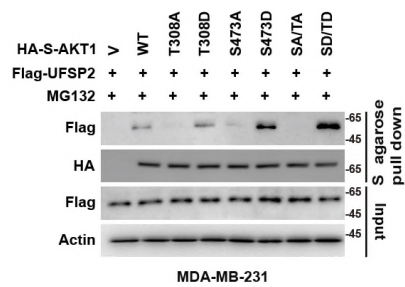
Supplementary Fig. 3a



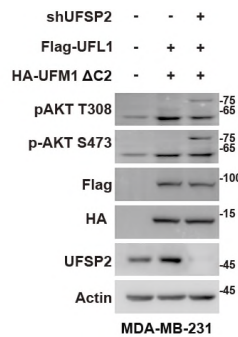
Supplementary Fig. 3m



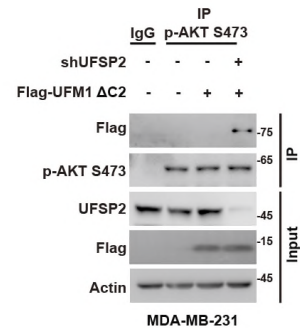
Supplementary Fig. 3r



Supplementary Fig. 3p



Supplementary Fig. 3q



**a**, MDA-MB-231 cells were transfected with the indicated plasmids and serum-starved for 16 h, followed by treatment with 100 nM insulin for indicated time periods before harvest. Cell lysates were pulled down using S-agarose, and then UFMylation and phosphorylation of HA-S-AKT1 were then examined. **m**, MDA-MB-231 cells stably expressing control or UFSP2 shRNA were transfected with the indicated plasmids and UFMylation of endogenous AKT1 was analyzed by immunoprecipitation with an anti-Flag antibody, followed by western blotting using an anti-AKT1 antibody. **r**, MDA-MB-231 cells were transfected with the indicated plasmids and treated with MG132 for 10 hours before harvest. Cell lysates were pulled down using S-agarose, and the interaction between AKT1 and UFSP2 was then examined. **p**, MDA-MB-231 cells were transfected with indicated plasmids, and Western blotting was performed. **q**, UFMylation of endogenous phosphorylated AKT1 (p-AKT S473) was analyzed by immunoprecipitation with an anti- p-AKT S473 antibody, followed by western blotting using an anti-Flag antibody in MDA-MB-231 cells with or without UFSP2 depletion and Flag-UFM1 ΔC2 overexpression.

+ UFMylation of AKT1 in TNBC context: The identification of AKT1 Lysines 189, 276 and 297 ufmylated by UFL1 is quite promising, however, Figure 2 i, j, k have been used human kidney cell line HEK293 is not appropriate in the claimed scope of TNBC, the authors must perform these experiments with TNBC cell lines such as MDA-MB-231 and HCC1806 as used in other experiments (Fig 1).

We thank the reviewer for this constructive comment. We would first like to clarify that the experiments shown in Fig. 3a and b (previously labeled as Fig. 2j and 2k in the original manuscript) were in fact performed in TNBC cell line HCC1806. The original labeling was unclear and may have led to a misunderstanding. This has now been corrected in the revised version.

In Supplementary Fig. 2c (previously labeled as Fig. 2i in the original manuscript), we showed that simultaneous mutation of K189R, K276R, and K297R (3KR) substantially reduced AKT1 UFMylation in HEK293T cells. To extend these findings to TNBC models, we generate plasmids stably expressing UFMylation machinery components (plv.6-GFP-UBA5/UFC1/UFL1/UFBP1 and plv.3-Flag-UFM1  $\Delta$ C2), co-transfected them with plv.5-HA-S-AKT1 WT or 3KR into MDA-MB-231 and HCC1806 cells, and confirmed that the 3KR mutant markedly reduced AKT1 UFMylation in both TNBC cell lines (Fig. 2i, j).

Furthermore, we repeated the experiments from Fig. 3a and b (originally Fig. 2j and k in the original manuscript) in MDA-MB-231 cells. Consistent with results in HCC1806, the 3KR mutant displayed reduced binding to mTOR/Rictor, enhanced interaction with PP2A-B55 $\alpha$ , and no significant effect on binding to PDK1, PP2A-B56 $\beta$ , or PHLPP1 (Supplementary Fig. 3e, h).

Together, these additional experiments validate that Lys189, Lys276, and Lys297 are key UFL1-mediated UFMylation sites of AKT1 in TNBC, thereby reinforcing the mechanistic relevance of our findings within the appropriate disease context.

Fig. 2i

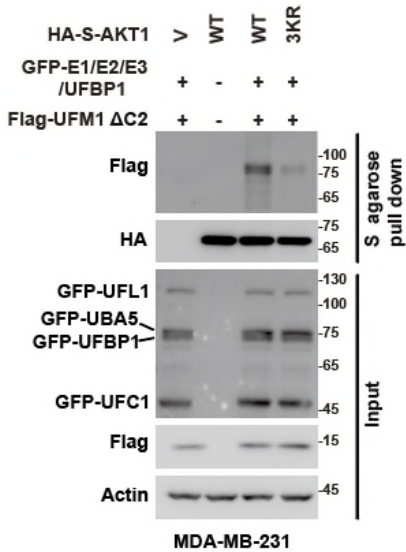
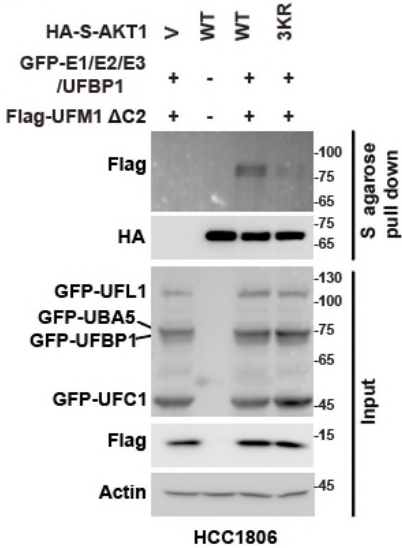
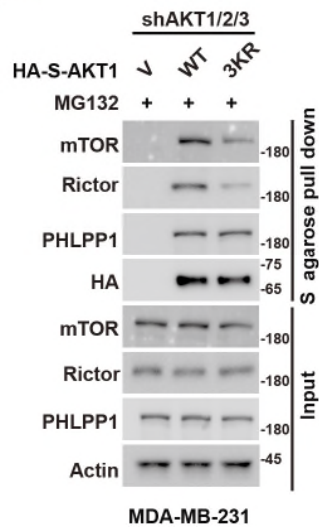


Fig. 2j

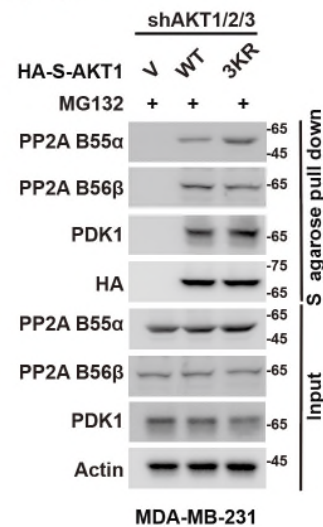


i, j, UFMylation assay of the HA-S-AKT1 WT and 3KR was performed in MDA-MB-231 and HCC1806 cells expressing the indicated components of the UFMylation system.

Supplementary Fig. 3e



Supplementary Fig. 3h



**e, h,** MDA-MB-231 cells were transfected with the indicated plasmids and treated with MG132 for 10 hours before harvest. Cell lysates were pulled down using S-agarose, and the interaction between AKT1 and the indicated proteins was then examined.

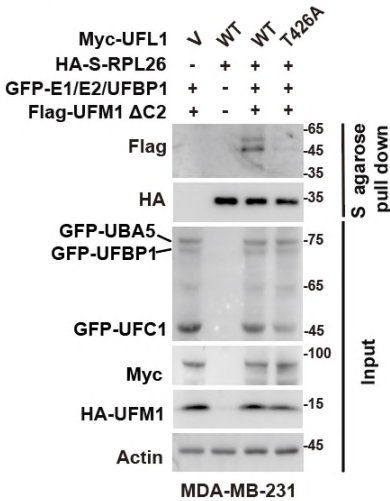
**+ Mechanistic insight for UFL1 T426 phosphorylation:** The data support AKT1-mediated phosphorylation of UFL1 at T426, but the downstream effect, i.e., how this modification structurally or functionally enhances UFL1's enzymatic activity—is still unclear with only connection with AKT1 phosphorylations and AKT downstream. The authors should provide additional biochemical or structural rationale, if available, or acknowledge this limitation and discuss potential mechanisms.

We thank the reviewer for this insightful comment regarding to the mechanistic consequence of UFL1 T426 phosphorylation. To address this issue, we examined whether this regulatory mode extends beyond a single substrate. UFMylation assays in MDA-MB-231 cells showed that the UFL1 T426A mutant significantly reduced the UFMylation of two established substrates, RPL26 and ERα<sup>5, 6</sup>, compared to wild-type UFL1 (Supplementary Fig. 4a, b). Moreover, during our revision process, an independent study reported that AKT directly phosphorylates UFL1 at T426 to promote UFMylation of ArPC4 and enhance lung cancer metastasis<sup>7</sup>. This independent finding is consistent with our results and suggest that AKT1-mediated phosphorylation of UFL1 at T426 may represent a general regulatory mechanism that enhances UFL1's ability to mediate UFMylation, likely through promoting efficient assembly of the UFMylation machinery complex or modulating its enzymatic activity.

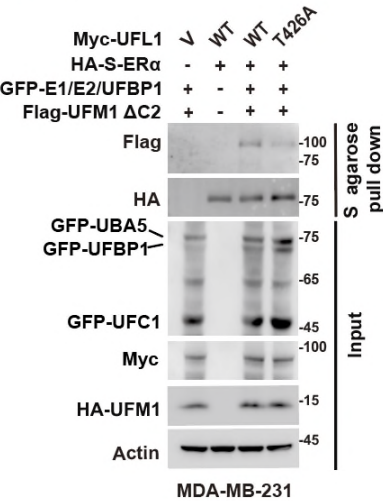
To further dissect the mechanism, we assessed whether T426 phosphorylation influences UFL1's interaction with other components of the UFMylation machinery. We found that either the T426A mutation or pharmacological inhibition of AKT by capivasertib significantly weakened UFL1's interaction with UFBP1 and CDK5RAP3, while not affecting its binding to UFC1 (Fig. 4i, j). Since T426 resides within the peptidyl transferase centre (PTC) loop of UFL1, a region implicated in regulating UFMylation complex assembly<sup>5</sup>, we propose that phosphorylation at T426 may induce conformational change in the PTC loop, thereby modulating UFBP1/CDK5RAP3 binding and promoting efficient complex assembly and enzymatic activity toward substrates.

While direct structural evidence is not yet available, our results together with recent literature, suggest that T426 phosphorylation may function as a conformational switch to facilitate UFMylation complex assembly and activity. We acknowledge this as a limitation of the current study and agree that future biochemical and structural analysis will be necessary to delineate the precise molecular mechanism.

Supplementary Fig. 4a



Supplementary Fig. 4b



**a**, UFMylation assay of the HA-S-RPL26 was examined in MDA-MB-231 cells co-transfected with the indicated UFMylation system components. **b**, UFMylation assay of the HA-S- ERα was examined in MDA-MB-231 cells co-transfected with the indicated UFMylation system components.

Fig. 4i

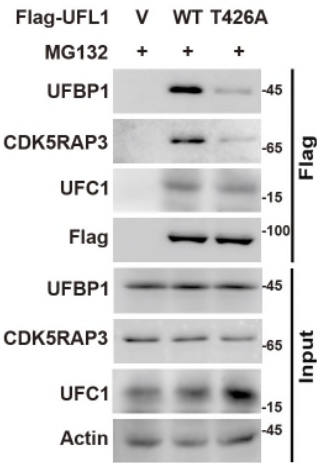
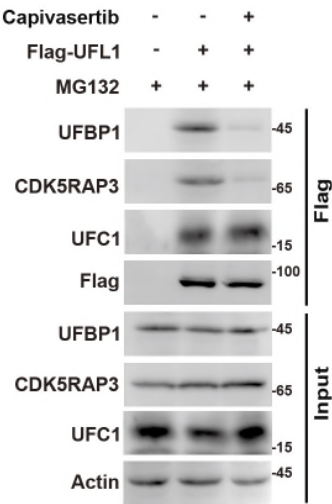


Fig. 4j



**i**, Cells were transfected with vector, Flag-UFL1 WT or T426A mutant and treated with MG132 for 10 hours before harvest. Cell lysates were subjected to immunoprecipitation with an anti-Flag antibody. Western blotting was performed using the indicated antibodies. **j**, Cells were transfected with vector or Flag-UFL1 and treated with capivasertib (10 μM) for 24 hours before harvest. Cell lysates were subjected to immunoprecipitation with an anti-Flag antibody. Western blotting was performed using the indicated antibodies.

+ Therapeutic characterization of PDAU-TAT: The PDAU-TAT peptide shows promising anti-tumor effects, but key pharmacological parameters (e.g., half-life, *in vivo* stability, biodistribution, immune tolerance) are not described or addressed. Please provide further data (if available) or discuss the limitations and future work needed to validate PDAU as a therapeutic agent.

We sincerely thank the reviewer for this valuable comments. In response, we have supplemented key pharmacological data and outlined future directions to strengthen the therapeutic characterization of PDAU.

We evaluated PDAU following both intravenous (IV) and intraperitoneal (IP) administrations. As shown in Table S1, S2 and Supplementary Fig. 5b, PDAU exhibited a mean half-life ( $t_{1/2z}$ ) of  $1.29 \pm 0.15$  h after IV administration—reflecting rapid systemic clearance typical of direct vascular delivery. Following IP administrations, PDAU displayed a longer mean half-life of  $3.74 \pm 0.94$  h, indicating a moderate circulation time *in vivo*. Although stability was not assessed independently, the consistent pharmacokinetic profiles across animals (e.g. AUC (0–t) mean of  $35.31 \mu\text{g/mL}\cdot\text{h}$  with SD of  $18.29 \mu\text{g/mL}\cdot\text{h}$ ) suggest appreciable *in vivo* stability.

For biodistribution, we tracked Cy5-labeled PDAU in tumor-bearing mice using *in vivo* imaging (Supplementary Fig. 5c). PDAU reached peak level at 8 h post administration, and *ex vivo* imaging confirmed PDAU distribution in tumors as well as multiple organs. By 24 h, PDAU was largely cleared, with residual signals in tumors and the liver (Supplementary Fig. 5d). These data indicate efficient tumor targeting and progressive systemic clearance, a favorable property for anti-tumor application, although potential off-target retention in the liver warrants further investigation.

We acknowledge that immune tolerance and long-term toxicity have not yet been systematically evaluated. In the future, we plan to optimize PDAU structure to improve its pharmacokinetic features and tumor specificity by incorporation of tumor-homing ligands or charge modifications. We will perform rigorous quantitative biodistribution study and conduct long-term toxicity and immunogenicity assessments. These strategies will be essential to refine PDAU's pharmacological profiles and balance efficacy with improved safety.

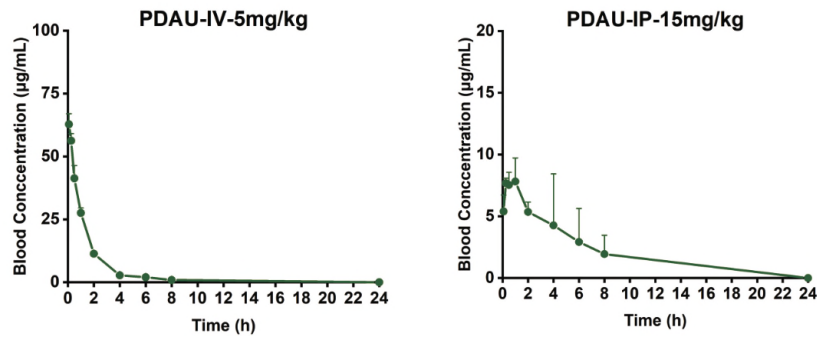
NO.	AUC <sub>(0-t)</sub>	AUC <sub>(0-∞)</sub>	MRT <sub>(0-t)</sub>	MRT <sub>(0-∞)</sub>	$t_{1/2z}$	Vz	CLz	C <sub>max</sub>
	h* $\mu\text{g/mL}$	h* $\mu\text{g/mL}$	h	h	h	mL/kg	mL/min/kg	$\mu\text{g/mL}$
1	87.78	90.35	1.33	1.58	1.31	104.88	0.922	67.61
2	85.55	86.33	1.30	1.38	1.13	94.47	0.965	60.75
3	84.51	86.26	1.53	1.70	1.43	119.88	0.966	60.04
Mean	85.95	87.65	1.39	1.55	1.29	106.41	0.951	62.80
SD	1.67	2.34	0.12	0.16	0.15	12.78	0.025	4.18

**Table S1. Pharmacokinetic Parameters after Intravenous Administration**

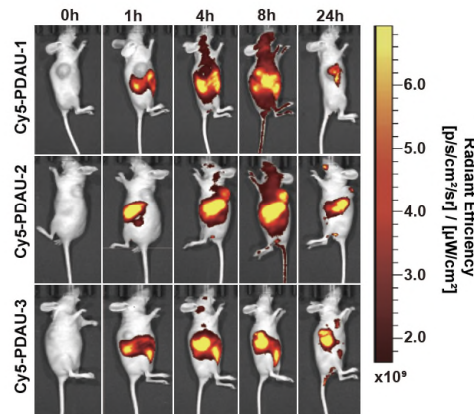
NO.	$AUC_{(0-t)}$	$AUC_{(0-\infty)}$	$MRT_{(0-t)}$	$MRT_{(0-\infty)}$	$t_{1/2z}$	$T_{max}$	$C_{max}$	$F$
	$\mu\text{g/mL}^*_{\text{h}}$	$\mu\text{g/mL}^*_{\text{h}}$	h	h	h	h	$\mu\text{g/mL}$	%
1	56.08	71.67	3.58	5.49	3.02	1.00	10.00	21.75
2	28.27	36.46	2.85	5.11	3.40	0.25	7.27	10.96
3	21.59	25.62	2.05	4.08	4.80	0.25	8.08	8.37
Mean	35.31	44.58	2.83	4.89	3.74	0.50	8.45	13.70
SD	18.29	24.08	0.76	0.73	0.94	0.43	1.40	7.09

**Table S2. Pharmacokinetic Parameters after Intraperitoneal Administration**

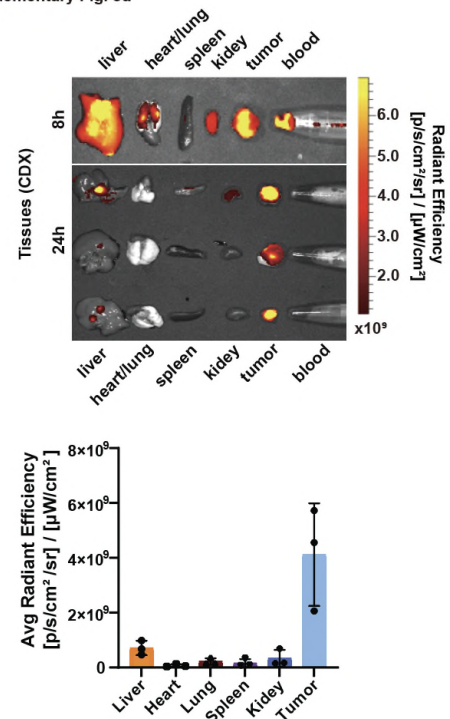
Supplementary Fig. 5b



Supplementary Fig. 5c



Supplementary Fig. 5d



**b**, Plasma concentration-vs-time profiles for PDAU in mice following intravenous (IV) administration at a dose of 5 mg/kg (left panel) or intraperitoneal (IP) administration at a dose of 15 mg/kg (right panel). Data represents blood concentration (µg/mL) measured at indicated time points. **c**, In vivo fluorescence imaging of mice at 0 h, 1 h, 4 h, 8 h, and 24 h after administration of Cy5-labeled PDAU (Cy5-PDAU). **d**, Ex vivo fluorescence imaging of major tissues and tumors harvested from mice at 8 h and 24 h post Cy5-PDAU administration. Quantitative analysis of fluorescence intensity in major tissues and tumors at 24 h.

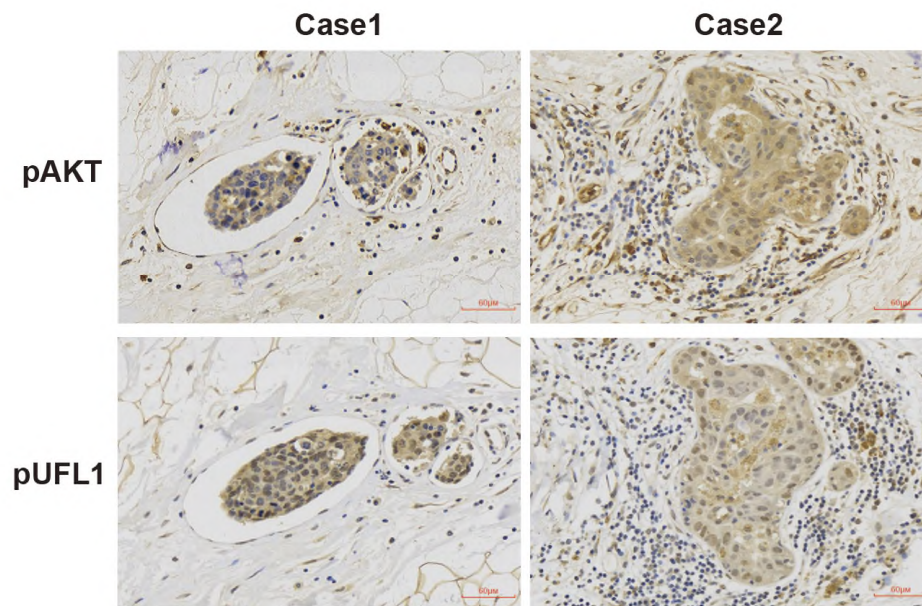
+ Quantification of IHC data: The IHC analysis linking pUFL1 and pAKT in Figure 6 is promising, but the scoring approach and representative images require further clarification. Please include a more detailed description of scoring methods and representative high-quality images in the supplementary data, and clarify how the correlation and regression line were generated. If outliers influence the result, a residual plot or alternative correlation analysis would be helpful for clarity.



We sincerely thank the reviewer for this constructive suggestion. In the revised manuscript, we have added a more detailed description of immunohistochemical (IHC) scoring method in the Methods section. Paraffin-embedded tissue sections were subjected to IHC staining, as previously described<sup>8</sup>. The final IHC score was determined by integrating two key parameters: the quantity score, representing the percentage of positively stained cells (0 = no immunostaining; 1 = 1-10% of cells showing positive staining; 2 = 11-50% of positive cells; 3 = 51-80% of positive cells; and 4 =  $\geq 81\%$  of positive cells) and the staining intensity score (0 =negative, 1=weak, 2=moderate, 3=strong). For each tissue section, the composite IHC score was calculated by multiplying the intensity score by the quantity score, resulting in a total score ranging from 0 to 12. Immunoreactivity was classified as strong (9-12), moderate (5-8), weak (1-4), or negative (0)<sup>9</sup>. For downstream data analysis, samples with IHC score of more than 6 were considered to be high, and less than 6 were considered to be low. We used GraphPad Prism to create a scatter plot with two quantitative variables, followed by linear correlation analysis to generate regression lines. The  $\chi^2$ -test (Fig. 6b) and the Pearson's correlation coefficient (Fig. 6c) were used for statistical analysis of the correlation between pUFL1 and pAKT.

Additionally, we have replaced the representative images in Figure 6a with higher-resolution versions to enhance data presentation.

**Fig. 6a**



**a, Representative IHC staining of pUFL1 and pAKT in TNBC (n=40).**

---

Minor points:

- + The Discussion is quite dense, please consider focusing more sharply on the most novel aspects.
- Figure legends should more consistently cross-reference supplementary figures and provide necessary experimental context (e.g., replicate numbers, statistical tests).



We sincerely thank the reviewer for this thoughtful suggestion. In the revised manuscript, we have streamlined the Discussion section to highlight the most novel aspects of our study.

Additionally, we have revised all figure legends to ensure consistency and clarity by cross-referencing relevant supplementary figures and including necessary experimental details on replicate numbers and statistical tests used in the experiments.

+ Please revise the manuscript for typo errors and awkward phrasing, particularly in the Methods section. We thank the reviewer for pointing out this issue. In the revised manuscript, we have carefully corrected typo errors and rephrased awkward or unclear sentences to improve readability and precision, with particular attention to the Methods section.

Reviewer #2 (Breast cancer, Remarks to the Author):

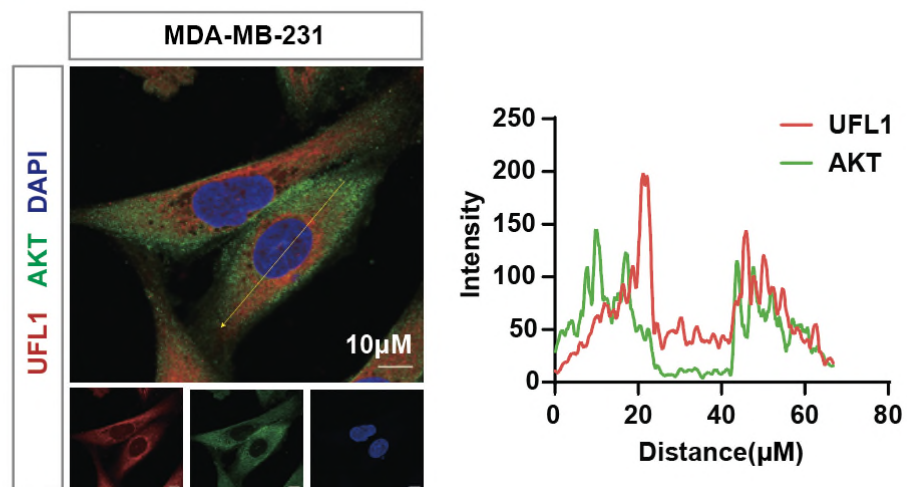
The manuscript "Targeting the UFL1-AKT Cascade Suppresses Triple Negative Breast Cancer Progression" by Yang, Wen and Ma et al., describes a new interesting positive feedback loop between AKT1 UFMylation and UFL1 phosphorylation. Following the identification of this link, the authors create a cell-penetrant peptide that blocks the interaction and leads to in vivo anti-tumour efficacy. Overall, the manuscript is well written and has a logical structure. I only have a few comments.

Major comments:

- If any conclusions are to be made from the IF experiment in Supp Fig 1e they should be repeated at much higher magnification, and co-localizations should be quantified.

We greatly appreciate the reviewer's constructive comment. In accordance with the suggestion, we repeated the immunofluorescence staining experiments using a higher magnification (63x, compared to the previous 40x) and quantified co-localization by pixel intensity analysis<sup>7</sup>. As shown in Supplementary Fig. 1f, UFL1 co-localized with AKT1 in MDA-MB-231 cells.

**Supplementary Fig. 1f**



f, Co-localization of endogenous UFL1(red) and AKT1(green) in MDA-MB-231 cells were detected by immunofluorescence (IF) staining. Nuclei were counterstained with DAPI. Scale bars, 10  $\mu$ m. The pixel intensity plot for the line was shown in the right panel.

- Along the same line. I understand that many of the IP experiments are hard to quantify, but the authors should provide quantification and statistics for all claims based on regular western blotting experiments (Fx Fig 1k and l, but many more).

We thank the reviewer for this valuable comment. In response, we have repeated all the relevant Western blotting experiments three independent times and performed quantitative statistics analysis accordingly. The quantified results are included in the revised figures where applicable or provided in Source Data File.

Minor comments:

- Figure 1i: I think MDA-MB-231 are missing in the figure?

We thank the reviewer for pointing this out. The experiments shown in Figure 1i were performed in HCC1806 cells. Specifically, we performed co-immunoprecipitation (Co-IP) assays to investigate the interaction between UFL1 and AKT. In these assays, we immunoprecipitated pan-AKT (upper left) or AKT1 (upper right) and detected UFL1 in the immunoprecipitates. Conversely, we immunoprecipitated UFL1 and detected pan-AKT (lower left) or AKT1 (lower right) in the immunoprecipitates. We have now clarified this in the revised manuscript to avoid confusion.

- Line 168: UFMylation of AKT1 was detected by a 20kDa shift compared to unmodified AKT1. This seems rather unspecific. Is it not possible to validate with alternate methods? Fx m/s?

We thank the reviewer for raising this important point. To address the concern regarding specificity, we provide additional evidence supporting the AKT1 UFMylation.

Firstly, when UFMylation machinery component plasmids were transfected in HEK293T (Fig. 2a) and TNBC cells (Fig. 2i, j), we observed the shifted band corresponding to UFMylated AKT1. This band was absent in cell without HA/Flag-UFM1  $\Delta$ C2 transfection, indicating that the shift specifically represents UFMylation. Secondly, immunoprecipitation of endogenous p-AKT S473 revealed a UFMylated AKT band only when the UFM1-specific protease UFM1-1 was depleted (Supplementary Fig. 3q), further supporting specificity. Thirdly, in both HEK293T and TNBC cells transfected with wild-type (WT) AKT1, we observed the shifted UFMylated band, while this band was absent in cells transfected with the 3KR mutant (Fig. 2i, j). This demonstrated that the shifted band depended on specific lysine residues (Lys189, Lys276, Lys297) and is unlikely to be a non-specific modification.

Regarding the reviewer's suggestion of alternative methods, we fully agree that mass spectrometry (MS) represents the gold standard for validating UFMylation sites. To address this, we immunoprecipitated AKT1 in HEK293 cells co-transfected with the UFMylation machinery plasmids and subjected the sample to MS analysis. However, no UFMylation sites were detected. During MS process, trypsin cleavage of UFM1 $\Delta$ C2-conjugated substrates leaves a valine-glycine (VG) remnant covalently linked to the  $\epsilon$ -amino group of Lys (VG- $\epsilon$ -K isopeptide), which differs from the diglycine (GG) remnant generated in ubiquitin modification. We

suspect the lack of a commercially available anti-VG-ε-K motif-specific antibody equivalent to the widely used anti-GG-ε-K antibody for ubiquitin remnant enrichment <sup>10</sup>, hindered enrichment and subsequent detection of UFMylated peptides. To overcome this limitation, we are generating the anti-VG-ε-K motif-specific antibody using a VG-ε-K peptide library in collaboration with Hangzhou Huaan Biotechnology Co., Ltd. We anticipate that this tool will enable enrichment and site-specific identification of UFMylated substrate in the future studies. Taken together, although technical limitations precluded direct MS-based site identification, our biochemical evidence strongly supported the conclusion that AKT1 undergoes UFMylation.

Fig. 2a

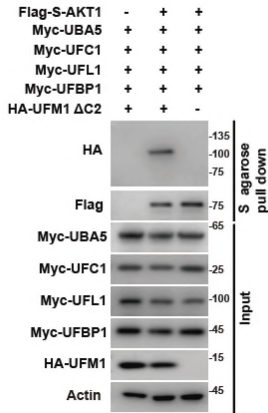


Fig. 2i

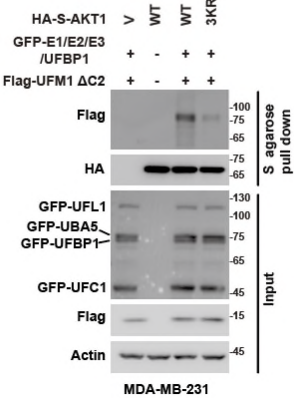
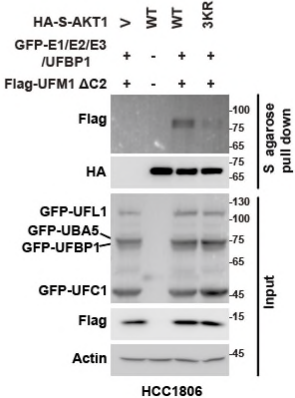
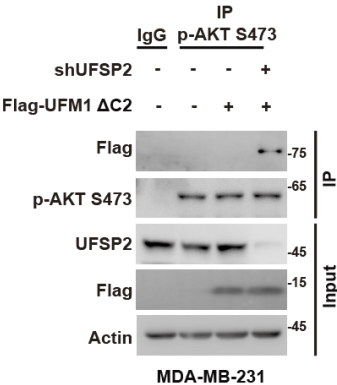


Fig. 2j



a, UFMylation of AKT1 was analyzed by western blotting using an anti-HA antibody in HEK293T cells transfected with Flag-S-AKT1 and the components of the UFMylation system (Myc-UBA5, Myc-UFC1, Myc-UFL1, Myc-UFBP1, HA-UFM1 ΔC2). i, j, UFMylation assay of HA-S-AKT1 WT and 3KR was performed in MDA-MB-231 and HCC1806 cells expressing the indicated components of the UFMylation system.

Supplementary Fig. 3q



q, UFMylation of endogenous phosphorylated AKT1 (p-AKT S473) was analyzed by immunoprecipitation with an anti- p-AKT S473 antibody, followed by western blotting using an anti-Flag antibody in MDA-MB-231 cells with or without UFSP2 depletion and Flag-UFM1 ΔC2 overexpression.

- Should the correlation plot in Fig. 6c not have 40 dots?

We thank the reviewer for this valuable comment. The correlation plot in Fig. 6c is based on 40 samples, however, some data points overlap because multiple samples received identical immunohistochemistry (IHC) scores for pUFL1 and pAKT, which makes the number of visible dots appear fewer. To improve clarity, we have updated the figure legend and Methods to explicitly describe the scoring methods and note the possibility of overlapping data point.

Paraffin-embedded tissue sections were subjected to immunohistochemical (IHC) staining, as previously described<sup>8</sup>. The final IHC score was determined by integrating two key parameters: the quantity score (reflecting the percentage of positively stained cells) and the staining intensity score. The quantity score was graded on a 0-4 scale: 0 = no immunostaining; 1 = 1-10% of cells showing positive staining; 2 = 11-50% of positive cells; 3 = 51-80% of positive cells; and 4 =  $\geq 81\%$  of positive cells. Staining intensity was assigned a score of 0 (negative), 1 (weak), 2 (moderate), or 3 (strong). For each tissue section, the composite IHC score was calculated by multiplying the intensity score by the quantity score, resulting in a total score ranging from 0 to 12. Immunoreactivity was further categorized based on this composite score: 9-12 = strong immunoreactivity; 5-8 = moderate immunoreactivity; 1-4 = weak immunoreactivity; and 0 = negative immunoreactivity<sup>9</sup>. For downstream data analysis, samples with IHC score of more than 4 were considered to be high, and less than 4 were considered to be low. We used GraphPad Prism to create a scatter plot with two quantitative variables, followed by linear correlation analysis to generate regression lines. The  $\chi^2$ -test and the Pearson's correlation coefficient were used for statistical analysis of the correlation between pUFL1 and pAKT.

**Reviewer #3 (Protein UFMylation, Remarks to the Author):**

The manuscript by Yang et al reports a novel finding of a positive feed-back loop between UFM1 E3 ligase UFL1 and AKT1 in triple negative breast cancer (TNBC) cells. The authors have demonstrated that UFL1-mediated UFMylation enhances AKT1 phosphorylation and activation, thereby promoting tumor progression and drug resistance. Disruption of the UFL1-AKT1 interaction by a specific peptide significantly inhibits tumor progression, suggesting that the UFL-AKT1 axis may serve as a novel therapeutic target for TNBC treatment. The study uncovers a novel relationship between UFMylation and AKT1 and expands current understanding of the role of UFMylation in tumor progression. Most experiments were well-designed and executed, and the conclusions were generally supported by the data. However, more mechanistic studies are needed to support the proposed working model. Further investigation of this novel interaction in UFMylation biology would broaden the scope of the current study.

**Specific comments:**

1. In Fig.1m and n, a group of 'vector+Capivaserib' should be included. The effect of Capivaserib on phosphorylation of AKT substrates should be examined as in Fig.1i.

We thank the reviewer for this constructive suggestion. In response, we have included the "vector+Capivasertib" group in Fig.1m and n and repeated the experiments accordingly. Furthermore, we examined the effect of Capivasertib in TNBC cell lines and observed that Capivasertib treatment reduced phosphorylation of AKT downstream substrates (Supplementary Fig. 1i). These additional experiments have been incorporated into the revised manuscript accordingly.

Fig. 1m

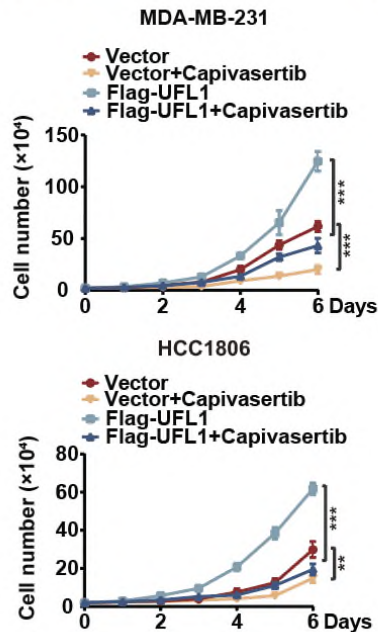
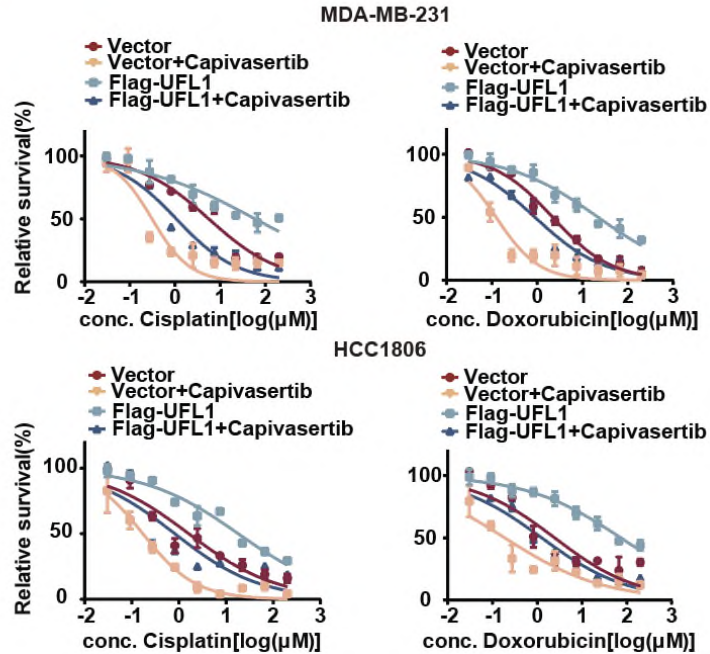
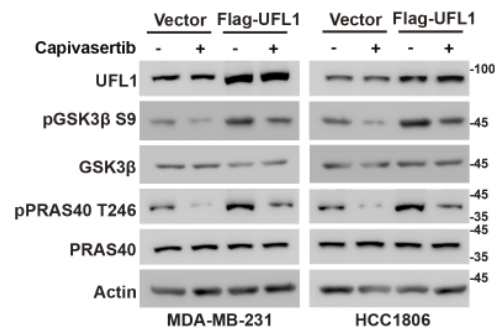


Fig. 1n



m, Cells were transfected with empty vector or Flag-UFL1 and treated with vehicle or capivasertib (1  $\mu$ M). Cell proliferation assay was performed. n, Cells were treated with DMSO or indicated concentrations of cisplatin or doxorubicin and cell survival was determined. Data showed as the mean  $\pm$  SD were analyzed by one-way ANOVA. \*\* $p$  < 0.01, \*\*\* $p$  < 0.001.

Supplementary Fig. 1i



I, MDA-MB-231 and HCC1806 cells were transfected with empty vector or Flag-UFL1 and treated with vehicle or capivasertib (10  $\mu$ M) for 24 hours before harvest. Western blotting was performed with indicated antibodies.

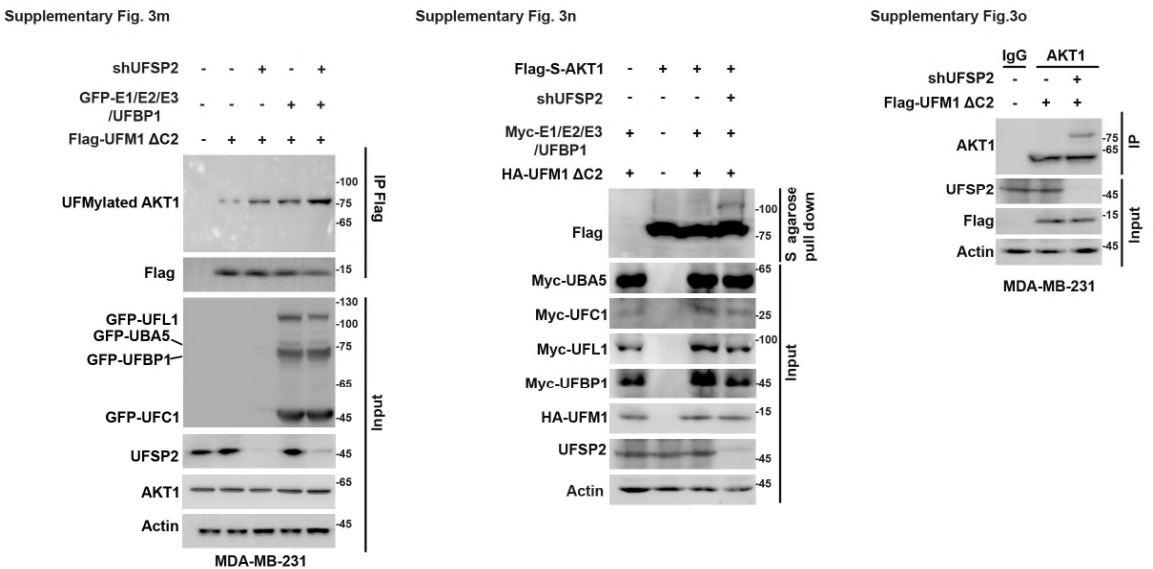
2. In Fig. 2a, does Flag antibody detect UFMylated AKT1? Similarly, does AKT antibody detect UFMylated form of endogenous AKT in Fig.2c? In Fig. 2, some UFMylated AKT1 were around 100 kD, while others were well below 100 kD marker. Please be consistent. Also please specify the cell line used in Fig. 2e, 2g, 2j and 2k.

We greatly appreciate the reviewer's constructive suggestion. Regarding antibody detection, we attempted to detect UFMylated AKT1 using Flag and AKT1 antibodies. However, these modified bands were not readily detected under conventional conditions. We propose that UFMylation of AKT1 may be a transient event, likely subject to coordinated regulation by de-UFMylation. Depletion of the UFM1-specific protease UFSP2 caused

a marked accumulation of UFMylated AKT1 in both control and UFMylation machinery components-transfected MDA-MB-231 cells (Supplementary Fig. 3m). Under the condition of UFSP2 knockdown, the accumulation of UFMylated AKT1 enabled detection of these modified forms with either Flag or AKT1 antibodies, thereby validating the specificity of the observed bands (Supplementary Fig. 3n, o).

Regarding the variation in molecular weights of UFMylated AKT1, these difference arose from the use of different AKT1 expression vectors across experiments. Our modified pIRES-FLAG-AKT1 produces a higher apparent molecular weight (around 15kDa) due to the tag encoded by the vector. While the absolute molecular weights varied accordingly, the relative mobility shift reflecting UFMylation was consistent across experiments.

We have clarified the cell line used in the revised figure and legends: Fig. 2e and g were performed in HEK293T, whereas Fig. 2j and k (noted as Fig. 3a and b in the revised manuscript) were performed in HCC1806 cells.



**m**, MDA-MB-231 cells stably expressing control or UFSP2 shRNA were transfected with the indicated plasmids and UFMylation of endogenous AKT1 was analyzed by immunoprecipitation with an anti-Flag antibody, followed by western blotting using an anti-AKT1 antibody. **n**, UFMylation of AKT1 was analyzed by western blotting using an anti-Flag antibody in HEK293T cells transfected with Flag-S-AKT1 and indicated plasmids. **o**, UFMylation of endogenous AKT1 was analyzed by immunoprecipitation with an anti-AKT1 antibody, followed by western blotting using an anti-AKT1 antibody in MDA-MB-231 cells stably expressing control or UFSP2 shRNA.

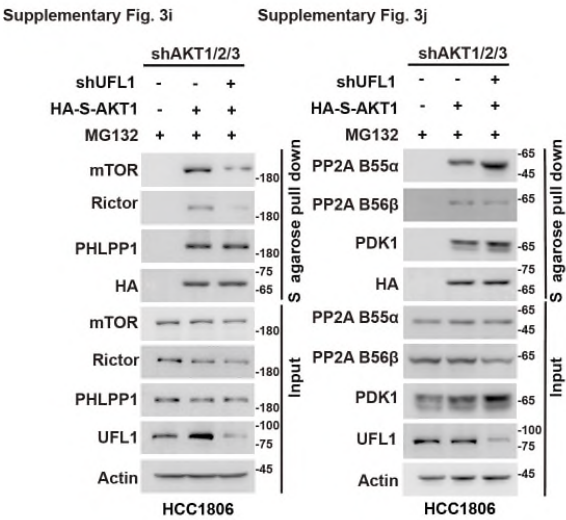
3. Fig. 3. It may be more appropriate to move Fig.2j and k to Fig. 3. Although AKT1 3KR mutant altered its interactions with the components of mTORC2 and PP2A complexes, it was not definitive evidence supporting the conclusion as claimed in the manuscript. It does not rule out the possibility that the mutation itself may affect the interaction. Therefore, more biochemical data may be needed to support the conclusion that happens to be the major point of the proposed working model. The authors should test the interaction



between AKT and its regulators in UFM1 or UFL1 depleted cells. Moreover, the authors should compare the interactions between UFMylated and unmodified AKT1 with its regulators in a more direct assay.

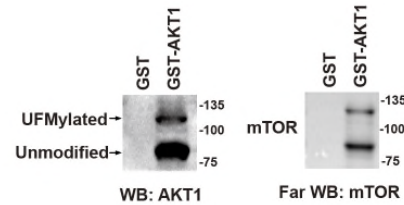
We sincerely appreciate the reviewer's constructive suggestions. In response, we have moved the original Fig. 2j and k to Fig. 3a and b in the revised manuscript to better align with the working model.

To address the concern that the 3KR mutation itself might influence interaction, we performed the following additional experiments. Firstly, we depleted UFL1 and transfected HA-S-AKT1 in HCC1806 cells to examine its interactions with mTORC2 and PP2A components. We found that UFL1 knockdown reduced the interaction between AKT1 and mTOR/Rictor, while enhancing the binding of PP2A B55α to AKT1 (Supplementary Fig. 3i, j). These findings are consistent with our earlier results and support a role of UFMylation in modulating AKT1 interactions. Secondly, to directly compare the binding abilities of UFMylated and unmodified AKT1, we performed Far-western blot assays using GST-AKT1 subjected to *in vitro* UFMylation reactions and SDS-PAGE (Supplementary Fig. 3h). Immobilized proteins on PVDF membranes were renatured to restore conformation and then incubated with purified Flag-mTOR. Quantitative analysis revealed that UFMylated AKT1 exhibited significantly stronger binding affinity to purified Flag-mTOR than unmodified AKT1 (Supplementary Fig. 3i). Together, these experiments provided additional biochemical evidence supporting our model that UFMylation enhances AKT1 interaction with components of mTORC2, thereby facilitating AKT activation.

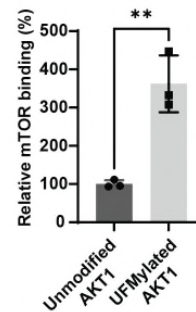


i, j, HCC1806 cells were transfected with the indicated plasmids and treated with MG132 for 10 hours before harvest. Cell lysates were pulled down using S-agarose, and the interaction between AKT1 and the indicated proteins was then examined.

Supplementary Fig. 3f



Supplementary Fig. 3g



f, Purified UFMylation components (His-UBA5, His-UFC1, His-UFL1, His-UFBP1 and His-UFM1  $\Delta$ C2) and GST-AKT1 were bacterially expressed and used for *in vitro* UFMylation reactions with GST-AKT1 as substrate. Reacted GST-AKT1 were separated by SDS-PAGE and transferred to PVDF membrane. After sequential denaturation/renaturation in guanidine-HCl buffers of decreasing concentration, membranes were incubated with Flag-mTOR purified from cells. Bound Flag-mTOR was detected by immunoblotting with anti-mTOR antibody. g, Quantitative analysis of relative mTOR binding ratio shows a significant increase in the interaction with UFMylated AKT1 compared to unmodified AKT. Results represent the mean  $\pm$  SD of three independent experiments. Data showed as the mean  $\pm$  SD were analyzed by one-way ANOVA. \*\* $p < 0.01$ .

4. Fig. 4. The finding of UFL1 phosphorylation by AKT is quite intriguing. It would be interesting to investigate the effect of this phosphorylation on overall UFMylation and other UFM1 targets such as RPL26 and ER $\alpha$ .

We thank the reviewer for this insightful comment regarding to the mechanistic consequence of UFL1 T426 phosphorylation. To address this, we examined whether this regulatory mode extends beyond a single substrate. UFMylation assays in MDA-MB-231 cells showed that the UFL1 T426A mutant significantly reduced the UFMylation of two established substrates, RPL26 and ER $\alpha$ <sup>5, 6</sup>, compared to wild-type UFL1 (Supplementary Fig. 4a, b). Moreover, during our revision process, an independent study reported that AKT directly phosphorylates UFL1 at T426 to promote UFMylation of ArPC4 and enhances lung cancer metastasis<sup>7</sup>. This independent finding is consistent with our results and suggest that AKT1-mediated phosphorylation of UFL1 at T426 may represent a general regulatory mechanisms that enhances UFL1's ability to mediate UFMylation, likely through promoting efficient assembly of the UFMylation machinery complex or modulating its enzymatic activity.

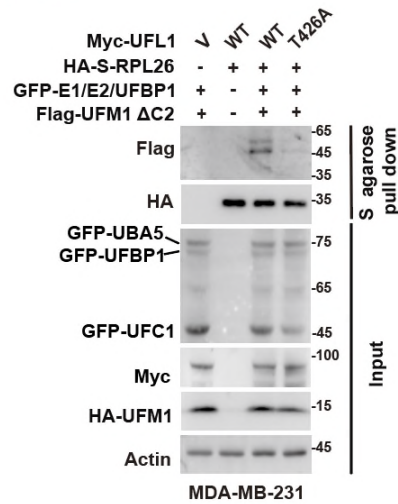
To further dissect the mechanism, we tested whether T426 phosphorylation influences UFL1's interaction with components of the UFMylation machinery. We found that either the T426A mutation or capivasertib treatment significantly weakened the interaction between UFL1 and UFBP1 and CDK5RAP3, while not affecting its binding to UFC1 (Fig. 4i, j). T426 resides within the peptidyl transferase centre (PTC) loop of UFL1, a region implicated in the UFMylation complex assembly<sup>5</sup>. We therefore propose that phosphorylation at T426 may induce conformational change in the PTC loop, thereby altering the accessibility of UFBP1/CDK5RAP3 binding and regulating complex assembly and enzymatic activity.

While direct structural evidence is currently lacking, our findings together with recent literature, suggest that T426 phosphorylation acts as a conformational switch to modulate UFMylation complex assembly and function.

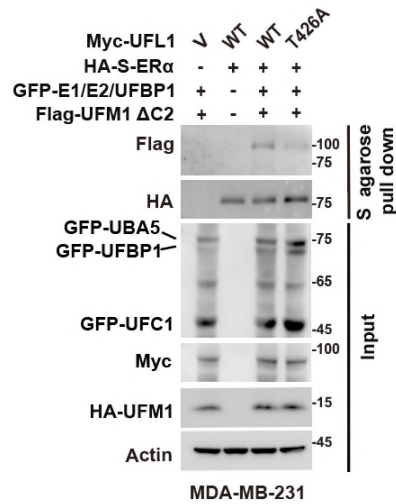


We acknowledge this limitation and agree that future biochemical and structural studies will be needed to define the precise molecular details of this regulatory mechanism.

Supplementary Fig. 4a



Supplementary Fig. 4b



**a**, UFMylation assay of the HA-S-RPL26 was examined in MDA-MB-231 cells co-transfected with the indicated UFMylation system components. **b**, UFMylation assay of the HA-S-ERα was examined in MDA-MB-231 cells co-transfected with the indicated UFMylation system components.

Fig. 4i

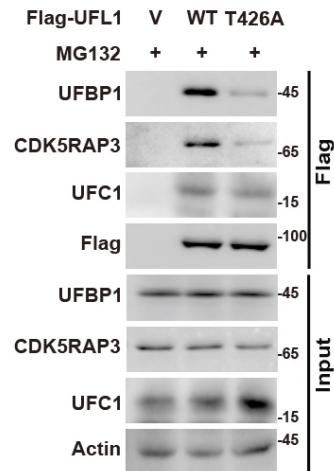
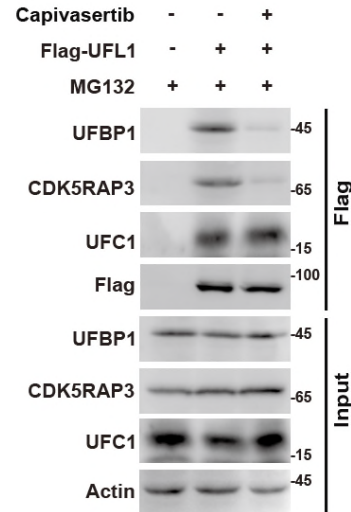


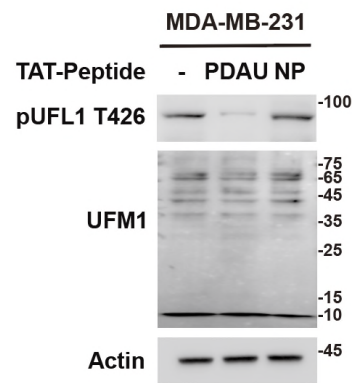
Fig. 4j



**i**, Cells were transfected with vector, Flag-UFL1 WT or T426A mutant and treated with MG132 for 10 hours before harvest. Cell lysates were subjected to immunoprecipitation with an anti-Flag antibody. Western blotting was performed using the indicated antibodies. **j**, Cells were transfected with vector or Flag-UFL1 and treated with capivasertib (10 μM) for 24 hours before harvest. Cell lysates were subjected to immunoprecipitation with an anti-Flag antibody. Western blotting was performed using the indicated antibodies.

5. Fig.5. The effect of PDAU on UFL1 phosphorylation and overall UFMylation should be examined. We sincerely appreciate the reviewer's constructive suggestions. To address this point, we treated TNBC cells with PDAU and assessed UFL1 phosphorylation and global UFMylation. We found that PDAU treatment markedly reduced phosphorylation of UFL1 at T426, but only modestly altered the overall UFMylation levels (Supplementary Fig. 5f). These results suggest that PDAU may selectively affect the UFMylation of certain substrates rather than broadly affecting all UFMylated proteins.

Supplementary Fig. 5f



f, MDA-MB-231 cells were treated with vehicle (ddH2O), PDAU or NP (10  $\mu$ M) for 24 hours and western blotting was performed indicated antibodies.

6. Fig.6. The observation of the correlation between pUFL1 and pAKT in TNBCs is interesting, but its clinical relevance is unclear. As suggested above, more experimental data are needed to back up the working model. Since AKT is the ultimate executioner to promote tumor progression in this model, what is the advantage of PDAU comparing to AKT inhibitors?

We sincerely appreciate the reviewer's insightful comments. To address the concern regarding PDAU's advantages over conventional AKT inhibitors, we emphasize both mechanistic selectivity and therapeutic safety, supported by our data and prior reports.

Clinically tested AKT inhibitors such as capivasertib have demonstrated efficacy in certain contexts but face major challenges, including limited selectivity, dose-limiting toxicity, tumor heterogeneity, and the lack of reliable biomarkers for treatment response<sup>11, 12</sup>. For instance, clinical studies have reported that capivasertib treatment is associated with significant adverse effects, including diarrhea in approximately 80% of patients, rash in 38%, and hyperglycemia in 16% of cases<sup>13-15</sup>, which limit compliance and dosing. Moreover, broad inhibition of AKT isoforms disrupts physiological functions in normal tissues, consistent with dose-dependent effects on glucose homeostasis observed in preclinical models<sup>15, 16</sup>.

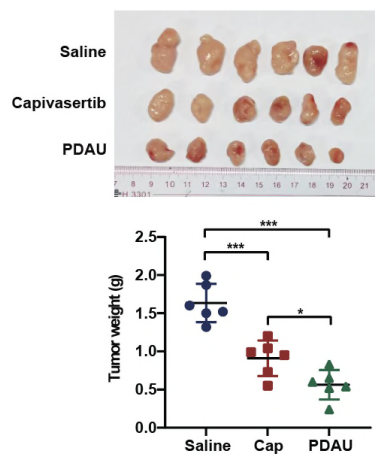
Our data suggest that PDAU achieves relatively better selectivity for tumor cells. PDAU effectively reduced phosphorylation of AKT downstream substrates (GSK3 $\beta$  Ser9 and PRAS40 Thr246) in TNBC cells, while exerting much weaker effects in non-tumorigenic MCF10A breast epithelial cells (Supplementary Fig. 5l). UFL1 expression is markedly upregulated in TNBC samples compared to normal breast tissues (Fig 1a, b). This finding is also validated in ER-positive breast cancer tissues<sup>17</sup>. However, compared with breast cancer cells, the protein level of UFL1 is relatively lower in MCF 10A cells (Supplementary Fig. 5m), and this may

indicate that PDAU exhibits lower toxicity toward normal cells. Thus, the strategy to disrupt UFL1-AKT interaction by PDAU may provide a wider therapeutic window and lower systemic toxicity than direct AKT inhibition.

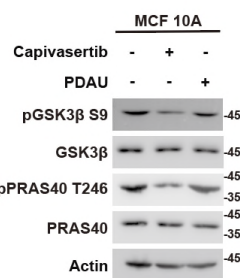
Mechanistically, PDAU acts upstream by disrupting UFL1-AKT interaction and UFL1-mediated regulation of AKT activation, rather than directly inhibiting kinase activity. Unlike ATP-competitive inhibitor that often trigger off-target and compensatory pathway activation and resistance, PDAU prevents AKT activation at its regulatory level, which may yield more durable suppression of AKT-driven tumor progression. Importantly, our *in vivo* data show that PDAU achieves stronger tumor growth inhibition than capivasertib in TNBC xenografts (Supplementary Fig.5k).

Together, our results demonstrate PDAU's potential clinical advantages over direct AKT inhibitors. By selectively targeting the UFL1-AKT axis in tumor cells, PDAU combines enhanced efficacy with reduced toxicity and a decreased risk of resistance, thereby supporting the clinical relevance of our working model and underscoring PDAU's translational potential in treatment of TNBC and other breast cancer subtypes with upregulated UFL1 and sustained AKT activation.

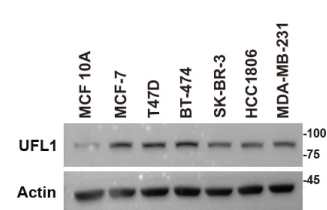
Supplementary Fig. 5k



Supplementary Fig. 5l



Supplementary Fig. 5m



**k**, HCC1806 cells ( $2 \times 10^6$ ) were subcutaneously implanted into nude mice ( $n = 6$ ). PDAU (15 mg/kg) was injected intraperitoneally every 2 days and capivasertib (100 mg/kg) was administered by oral gavage once daily for 5 days a week when tumor volume reached  $100 \text{ mm}^3$ . Tumors were harvested at endpoint and weighed (means  $\pm$  SD). Results represent the mean  $\pm$  SD from six mice. **l**, MCF 10A cells were treated with vehicle, capivasertib (10  $\mu\text{M}$ ) or PDAU (10  $\mu\text{M}$ ) for 24 hours and western blotting was performed indicated antibodies. **m**, Western Blot analysis of UFL1 protein expression in various breast cell lines including MCF 10A, and breast cancer cell lines MCF-7, T47D, BT-474, SK-BR-3, HCC1806, and MDA-MB-231. Data showed as the mean  $\pm$  SD were analyzed by one-way ANOVA.  $*p < 0.05$ ,  $***p < 0.001$ .

Reviewer #4 (Cell penetrating peptides, Remarks to the Author):

In this manuscript, Liu and colleagues reported a positive feedback loop between UFL1 and AKT through UFL1-mediated UFMylation of AKT1 and AKT-mediated phosphorylation. The loop results in a sustained activation of both pro-oncogenic regulators, the disruption of which inhibits TNBC progression. They also demonstrate that high level of UFL1 phosphorylation is associated with increased AKT phosphorylation in clinical samples. Overall, the work provides new insights into drug resistance of TNBC. However, more evidence is required before the publication. Detailed comments are listed below.

1. The authors have successfully proved that UFL1 has direct interaction with AKT1. They also generate mutants to map the sites that may influence UFMylation of AKT1. The authors may consider to identify UFMylated peptide fragments of AKT1 using mass spectrometry.

We thank the reviewer for raising this important point. We fully agree that mass spectrometry (MS) represents the gold standard for validating UFMylation sites of AKT1. To this end, we immunoprecipitated AKT1 in HEK293 cells co-transfected with the UFMylation machinery component plasmids and subjected the sample to mass spectrometry. However, no UFMylation sites were detected. During MS process, trypsin cleavage of UFM1 $\Delta$ C2-conjugated substrates leaves a valine–glycine (VG) remnant covalently linked to the  $\epsilon$ -amino group of Lys (VG- $\epsilon$ -K isopeptide), which differs from the diglycine (GG) remnant generated in ubiquitin modification. We suspect the lack of a commercially available anti-VG- $\epsilon$ -K motif-specific antibody equivalent to the widely used anti-GG- $\epsilon$ -K antibody for ubiquitin remnant enrichment<sup>10</sup>, hindered enrichment and subsequent detection of UFMylated peptides. To overcome this limitation, we are generating the anti-VG- $\epsilon$ -K motif-specific antibody using a VG- $\epsilon$ -K peptide library in collaboration with Hangzhou Huaan Biotechnology Co., Ltd. We anticipate that this tool will enable enrichment and site-specific identification of UFMylated substrate in the future studies. Taken together, although technical limitations precluded direct MS-based site identification, our biochemical evidence strongly supported the conclusion that AKT1 undergoes UFMylation.

To address the concern regarding specificity, we provide additional evidence supporting the UFMylation of AKT1. Firstly, when UFMylation machinery component plasmids were transfected in HEK293T (Fig. 2a) and TNBC cells (Fig. 2i, j), we observed the shifted band corresponding to UFMylated AKT1. This band was absent in cell without HA/Flag-UFM1  $\Delta$ C2 transfection, indicating that the shift specifically represents UFMylation. Secondly, immunoprecipitation of endogenous p-AKT S473 revealed a UFMylated AKT band only when the UFM1-specific protease UFSP2 was depleted (Supplementary Fig. 2g), further supporting specificity. Thirdly, in both HEK293T and TNBC cells transfected with wild-type (WT) AKT1, we observed the shifted UFMylated band, while this band was absent in cells transfected with the 3KR mutant (Fig. 2i, j). This demonstrated that the shifted band depended on specific lysine residues (Lys189, Lys276, Lys 297) and is unlikely to be a non-specific modifications.

Taken together, although technical challenges prevented MS-based site identification, the combined biochemical evidence strongly supported that AKT1 undergoes site-specific UFMylation.

2. In addition, the authors showed that K189, K276 and K297 are sites of UFMylation. A discussion on the influence of UFMylation on protein conformation, binding or further modification should be discussed. Since the molecular structure of human AKT1 has been published, a structure-based discussion may be helpful.

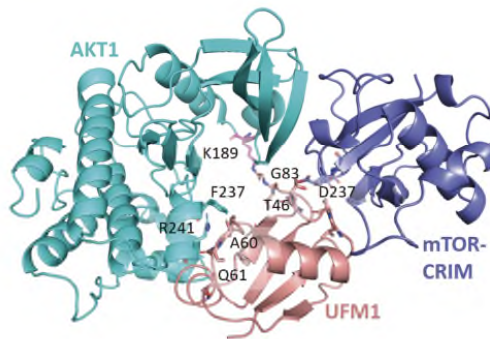
We sincerely appreciate the reviewer's insightful suggestion. In response, we incorporated structure-based modeling to provide mechanistic context for how UFMylation may influence AKT1 regulation.

Using AlphaFold3-based modeling, we examined AKT1-B55 $\alpha$  interaction. UFMylated AKT1 were modeled in maestro (Schrödinger, LLc, New York, NY, 2024), with UFM1 derived from the crystal structure (PDB ID:5IA7), conjugated via its terminal Gly83 to K189 of AKT1. Thr308-phosphorylated AKT1 is a substrate of PP2A-B55 $\alpha$ , the substrate-recognizing subunit of the PP2A complex<sup>18</sup>. Modeling suggests that UFMylation at Lys189, Lys276 and Lys297 introduces substantial steric hindrance that could disrupt B55 $\alpha$  engagement, thereby impairing AKT1 dephosphorylation (Supplementary Fig. 3l).

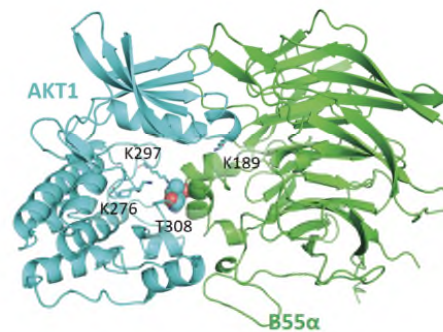
We further modeled the AKT1/CRIM-SIN1 complex structures using AlphaFold3 (Supplementary Fig. 3k). Here, the UFM1 Ala60 and Ala 61 formed stabilizing contacts with AKT1 residues Phe237 and Arg241, while UFM1 residues Ala45 and Thr46 interacted with Asp237 and Ser260 within the CRIM domain of SIN1, a key mTORC2 subunit mediating substrate specificity and complex stability<sup>19</sup>. These interactions suggest that UFMylation might generate an additional interface bridging AKT1 and SIN1, thereby enhancing substrate recruitment and promoting efficient phosphorylation of AKT1 at S473 by mTORC2. Given the structural complexity of mTORC2, however, we cannot exclude the possibility that AKT1 UFMylation also engages other subunits of the mTORC2 complex, which warrants further investigation.

Together, these structural models support a dual mechanism whereby UFMylation facilitates AKT1 phosphorylation by mTORC2 while simultaneously restricting dephosphorylation by PP2A. While structural predictions provide valuable insights, we acknowledge that biochemical and structural studies will be needed to definitely validate these precise mechanisms.

Supplementary Fig. 3k



Supplementary Fig. 3l

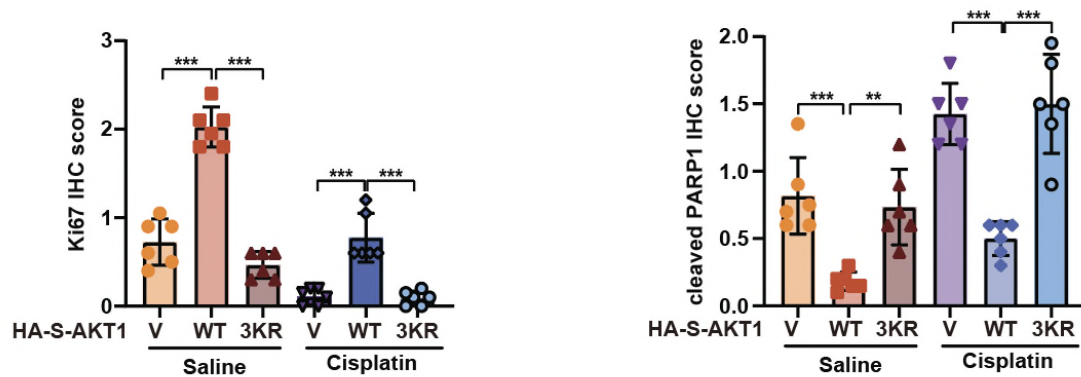


**k**, Overall structure of the AKT1 (cyan)/mTOR-CRIM (dark blue) complex with UFM1 (pink). **l**, Overall structure of the AKT1 (cyan)-B55 $\alpha$  (green) complex.

3. In Figure 3f, a semi-quantification of the levels of Ki67 and cleaved PARP1 should be performed.

We thank the reviewer for this helpful suggestion. As advised, we performed semi-quantification of Ki67 and cleaved PARP1 levels, now presented in Fig. 3g (previously labeled as Fig. 3f in the original manuscript), and incorporated the quantitative data into the revised manuscript.

Fig. 3g



g, IHC staining and quantification of Ki67 and cleaved PARP1 expression in a subcutaneous tumor model (n=6) from (e). Data showed as the mean ± SD were analyzed by one-way ANOVA. \*\* $p < 0.01$ , \*\*\* $p < 0.001$ .

4. The authors found that Thr426 was phosphorylated by AKT1. Mass spectrometry should be used to confirm this finding and to explore whether there is additional site of phosphorylation.

We sincerely thank the reviewer for this constructive suggestion. We fully agree that mass spectrometry (MS) is considered the gold standard for site validation. At the same time, we believe that in the present context, the combination of multiple orthogonal lines of evidence, together with independent external studies, provides strong and specific support for AKT1-mediated phosphorylation of UFL1 at Thr426, even in the absence of direct MS confirmation.

Firstly, phosphorylation of Flag-S-UFL1 in HCC1806 cells was detected using a phospho-AKT substrate antibody, and this signal was abolished upon AKT inhibition with capivasertib (Fig. 4b, c). Secondly, a phospho-specific antibody against pUFL1(T426) were generated, which confirmed phosphorylation in WT UFL1 but not in the phosphorylation-deficient T426A mutant (Fig. 4e). Consistently, capivasertib treatment or depletion of AKT1/2/3 significantly reduced T426 phosphorylation detected by this phospho-specific antibody (Fig. 4f, g), further confirming the AKT-mediated phosphorylation at T426. Thirdly, phosphorylation of UFL1 at T426 enhanced UFL1's interaction with UFBP1 and CDK5RAP3, increased UFMylation activity, and promoted AKT downstream signaling, all of which were markedly impaired by the T426A mutation or under AKT inhibition (Fig. 4i-k and Supplementary Fig. 4c). Finally, during our revision process, an independent study recently reported that AKT directly phosphorylate UFL1 at T426 to promote UFMylation of ArPC4<sup>7</sup>, further validating our findings.

Taken together, this evidence strongly support the conclusion that UFL1 Thr426 is phosphorylated by AKT1 and this event is functionally relevant. We fully acknowledge that targeted MS-based phosphoproteomic analyses would provide additional confirmation and may uncover additional phosphorylation sites, which we plan to pursue in future studies.



Fig. 4i

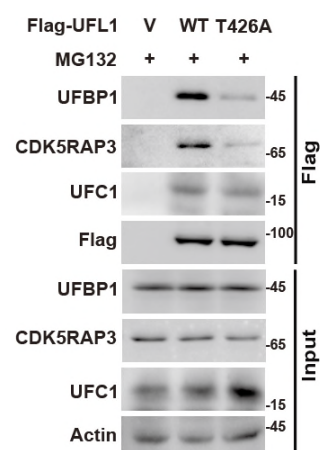
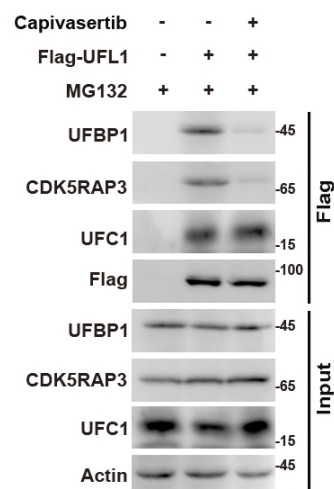


Fig. 4j



i, Cells were transfected with vector, Flag-UFL1 WT or T426A mutant and treated with MG132 for 10 hours before harvest. Cell lysates were subjected to immunoprecipitation with an anti-Flag antibody. Western blotting was performed using the indicated antibodies. j, Cells were transfected with vector or Flag-UFL1 and treated with capivasertib (10  $\mu$ M) for 24 hours before harvest. Cell lysates were subjected to immunoprecipitation with an anti-Flag antibody. Western blotting was performed using the indicated antibodies.

5. Peptide derived from UFL1 20-30 was developed as an antagonist that disrupt interaction between UFL1 and AKT. The K<sub>d</sub> of PDAU should be determined to quantify the affinity of the resulting peptide to AKT, using WT UFL1 and NP as controls. In addition, the distribution of PDAU in the tumors and other organs should be quantified.

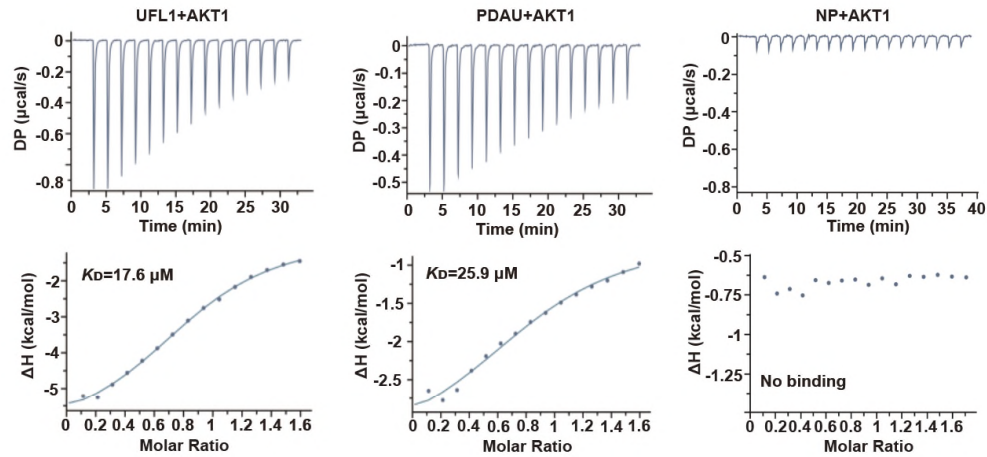
We sincerely appreciate the reviewer's insightful comments.

To quantify the binding affinity of PDAU to AKT1, we performed isothermal titration calorimetry (ITC) using UFL1 WT and NP as controls. UFL1 WT and PDAU bound to AKT1 with K<sub>D</sub> values of 17.6  $\mu$ M and 25.9  $\mu$ M, respectively, whereas NP exhibited no detectable binding (Supplementary Fig. 5a). These results confirm that PDAU directly interacts with AKT1 with measurable affinity, comparable to WT UFL1. The affinity of PDAU for AKT1 is modest, as expected for an unoptimized linear peptide. Consistent with previous reports, linear peptides derived directly from protein–protein interaction interfaces typically display micromolar affinities, as they capture only part of the binding interface and lack conformational constraints<sup>20, 21</sup>. Future optimization strategies such as cyclization, hydrocarbon stapling, and D-amino acid substitution are expected to improve both stability and affinity by enhancing peptide conformation, proteolytic resistance, and binding strength<sup>22</sup>.

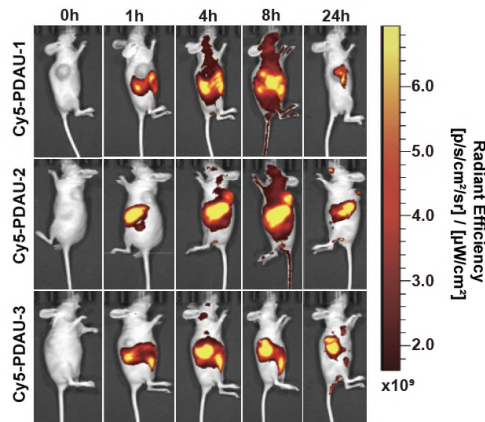
For biodistribution, we tracked Cy5-labeled PDAU in tumor-bearing mice using *in vivo* imaging (Supplementary Fig. 5c). PDAU reached peak level at 8 h post administration, and *ex vivo* imaging confirmed PDAU distribution in tumors as well as multiple organs. By 24 h, PDAU was largely cleared, with residual signals in tumors and the liver (Supplementary Fig. 5d). These data indicate efficient tumor targeting and progressive systemic

clearance, a favorable property for anti-tumor application, although potential off-target retention in the liver warrants further investigation.

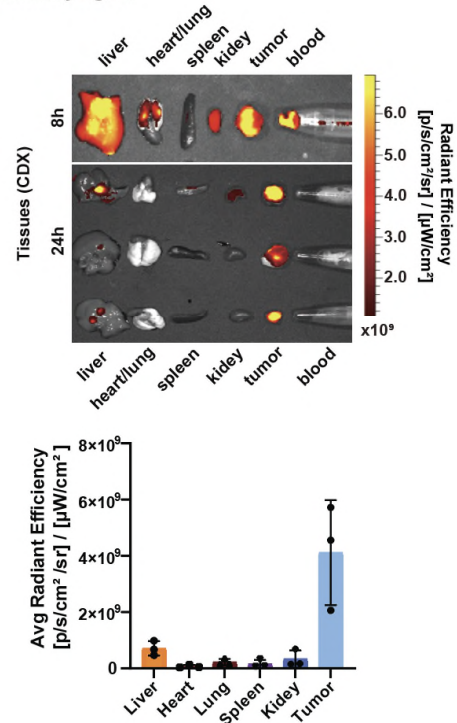
Supplementary Fig. 5a



Supplementary Fig. 5c



Supplementary Fig. 5d



**a**, Isothermal titration calorimetry (ITC) measurements showing the binding affinity of AKT1 with UFL1, PDAU and NP. DP, differential power; ΔH, enthalpy change. **c**, In vivo fluorescence imaging of mice at 0 h, 1 h, 4 h, 8 h, and 24 h after administration of Cy5-labeled PDAU (Cy5-PDAU). **d**, Ex vivo fluorescence imaging of major tissues and tumors harvested from mice at 8 h and 24 h post Cy5-PDAU administration. Quantitative analysis of fluorescence intensity in major tissues and tumors at 24 h.



6. The efficacy and safety of PDAU and AKT inhibitor capivasertib should be compared directly to demonstrate the potential application of modulating the discovered protein-protein interaction.

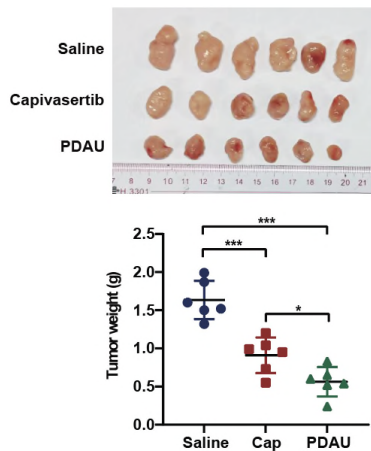
We sincerely appreciate the reviewer's insightful comments. To directly compare PDAU with capivasertib, we emphasized both efficacy and safety profiles supported by our supplementary data and relevant literature. Clinically tested AKT inhibitors such as capivasertib have demonstrated efficacy in certain contexts but face major challenges, including limited selectivity, dose-limiting toxicity, tumor heterogeneity, and the lack of reliable biomarkers for treatment response<sup>11, 12</sup>. For instance, clinical studies have reported that capivasertib treatment is associated with significant adverse effects, including diarrhea in approximately 80% of patients, rash in 38%, and hyperglycemia in 16% of cases<sup>13-15</sup>, which limit compliance and dosing. Moreover, broad inhibition of AKT isoforms disrupts physiological functions in normal tissues, consistent with dose-dependent effects on glucose homeostasis observed in preclinical models<sup>15, 16</sup>.

Our data suggest that PDAU achieves relatively better selectivity for tumor cells. PDAU effectively reduced phosphorylation of AKT downstream substrates (GSK3 $\beta$  Ser9 and PRAS40 Thr246) in TNBC cells, while exerting much weaker effects in non-tumorigenic MCF10A breast epithelial cells (Supplementary Fig. 5l). UFL1 expression is markedly upregulated in TNBC samples compared to normal breast tissues (Fig 1a, b). This finding is also validated in ER-positive breast cancer tissues<sup>17</sup>. However, compared with breast cancer cells, the protein level of UFL1 is relatively lower in MCF 10A cells (Supplementary Fig. 5m), and this may indicate that PDAU exhibits lower toxicity toward normal cells. Thus, the strategy to disrupt UFL1-AKT interaction by PDAU may provide a wider therapeutic window and lower systemic toxicity than direct AKT inhibition.

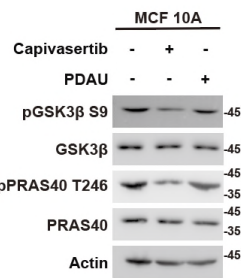
Mechanistically, PDAU acts upstream by disrupting UFL1-AKT interaction and UFL1-mediated regulation of AKT activation, rather than directly inhibiting kinase activity. Unlike ATP-competitive inhibitor that often trigger off-target and compensatory pathway activation and resistance, PDAU prevents AKT activation at its regulatory level, which may yield more durable suppression of AKT-driven tumor progression. Importantly, our *in vivo* data show that PDAU achieves stronger tumor growth inhibition than capivasertib in TNBC xenografts (Supplementary Fig.5k).

Together, our results demonstrate PDAU's potential clinical advantages over direct AKT inhibitors. By selectively targeting the UFL1-AKT axis in tumor cells, PDAU combines enhanced efficacy with reduced toxicity and a decreased risk of resistance, thereby supporting the clinical relevance of our working model and underscoring PDAU's translational potential in treatment of TNBC and other breast cancer subtypes with upregulated UFL1 and sustained AKT activation.

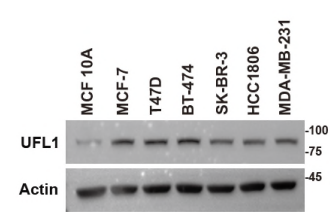
Supplementary Fig. 5k



Supplementary Fig. 5l



Supplementary Fig. 5m



**k**, HCC1806 cells ( $2 \times 10^6$ ) were subcutaneously implanted into nude mice ( $n=6$ ). PDAU (15 mg/kg) was injected intraperitoneally every 2 days and capivasertib (100 mg/kg) was administered by oral gavage once daily for 5 days a week when tumor volume reached  $100 \text{ mm}^3$ . Tumors were harvested at endpoint and weighed (means  $\pm$  SD). Results represent the mean  $\pm$  SD from six mice. **l**, MCF 10A cells were treated with vehicle, capivasertib (10  $\mu\text{M}$ ) or PDAU (10  $\mu\text{M}$ ) for 24 hours and western blotting was performed indicated antibodies. **m**, Western Blot analysis of UFL1 protein expression in various breast cell lines including MCF 10A, and breast cancer cell lines MCF-7, T47D, BT-474, SK-BR-3, HCC1806, and MDA-MB-231. Data showed as the mean  $\pm$  SD were analyzed by one-way ANOVA.  $*p < 0.05$ ,  $***p < 0.001$ .

## References

1. Chan, C.H. *et al.* The Skp2-SCF E3 ligase regulates Akt ubiquitination, glycolysis, herceptin sensitivity, and tumorigenesis. *Cell* **149**, 1098-1111 (2012).
2. Li, R. *et al.* Akt SUMOylation regulates cell proliferation and tumorigenesis. *Cancer Res* **73**, 5742-5753 (2013).
3. Gareau, J.R. & Lima, C.D. The SUMO pathway: emerging mechanisms that shape specificity, conjugation and recognition. *Nature reviews. Molecular cell biology* **11**, 861-871 (2010).
4. Bu, L. *et al.* PTEN suppresses tumorigenesis by directly dephosphorylating Akt. *Signal transduction and targeted therapy* **6**, 262 (2021).
5. DaRosa, P.A. *et al.* UFM1 E3 ligase promotes recycling of 60S ribosomal subunits from the ER. *Nature* **627**, 445-452 (2024).
6. Yoo, H.M. *et al.* Modification of ASC1 by UFM1 is crucial for ER $\alpha$  transactivation and breast cancer development. *Molecular cell* **56**, 261-274 (2014).
7. Zhao, K. *et al.* Akt-phosphorylated UFL1 UFMylates ArpC4 to promote metastasis. *Nature structural & molecular biology* **32**, 1528-1541 (2025).
8. Guan, T. *et al.* Phosphorylation of USP29 by CDK1 Governs TWIST1 Stability and Oncogenic Functions. *Advanced science (Weinheim, Baden-Wurttemberg, Germany)* **10**, e2205873 (2023).
9. Luo, K. *et al.* USP49 negatively regulates tumorigenesis and chemoresistance through FKBP51-AKT signaling. *Embo j* **36**, 1434-1446 (2017).

10. Zhou, J. *et al.* Dysregulation of PD-L1 by UFMylation imparts tumor immune evasion and identified as a potential therapeutic target. *Proc Natl Acad Sci U S A* **120**, e2215732120 (2023).
11. Huang, J. *et al.* Targeting the PI3K/AKT/mTOR Signaling Pathway in the Treatment of Human Diseases: Current Status, Trends, and Solutions. *J Med Chem* **65**, 16033-16061 (2022).
12. Okuzumi, T. *et al.* Inhibitor hijacking of Akt activation. *Nature chemical biology* **5**, 484-493 (2009).
13. Burstein, H.J., DeMichele, A., Fallowfield, L., Somerfield, M.R. & Henry, N.L. Endocrine and Targeted Therapy for Hormone Receptor-Positive, Human Epidermal Growth Factor Receptor 2-Negative Metastatic Breast Cancer-Capivasertib-Fulvestrant: ASCO Rapid Recommendation Update. *Journal of clinical oncology : official journal of the American Society of Clinical Oncology* **42**, 1450-1453 (2024).
14. Howell, S.J. *et al.* Fulvestrant plus capivasertib versus placebo after relapse or progression on an aromatase inhibitor in metastatic, oestrogen receptor-positive, HER2-negative breast cancer (FAKTION): overall survival, updated progression-free survival, and expanded biomarker analysis from a randomised, phase 2 trial. *Lancet Oncol* **23**, 851-864 (2022).
15. Chu, A., Hakami-Majd, N. & Whall, J.O. Acute hyperglycemic hyperosmolar syndrome associated with capivasertib, a new, oral targeted therapy for advanced breast cancer. *The American journal of emergency medicine* **88**, 273.e275-273.e277 (2025).
16. Turner, N.C. *et al.* Capivasertib in Hormone Receptor-Positive Advanced Breast Cancer. *The New England journal of medicine* **388**, 2058-2070 (2023).
17. Yoo, H.M., Park, J.H., Kim, J.Y. & Chung, C.H. Modification of ER $\alpha$  by UFM1 Increases Its Stability and Transactivity for Breast Cancer Development. *Molecules and cells* **45**, 425-434 (2022).
18. Kuo, Y.C. *et al.* Regulation of phosphorylation of Thr-308 of Akt, cell proliferation, and survival by the B55alpha regulatory subunit targeting of the protein phosphatase 2A holoenzyme to Akt. *J Biol Chem* **283**, 1882-1892 (2008).
19. Scaiola, A. *et al.* The 3.2-Å resolution structure of human mTORC2. *Science advances* **6** (2020).
20. Zhang, Y. *et al.* BTApep-TAT peptide inhibits ADP-ribosylation of BORIS to induce DNA damage in cancer. *Mol Cancer* **21**, 158 (2022).
21. Xiao, M.C. *et al.* TRIB3-TRIM8 complex drives NAFLD progression by regulating HNF4 $\alpha$  stability. *Journal of hepatology* **80**, 778-791 (2024).
22. Fang, P., Pang, W.K., Xuan, S., Chan, W.L. & Leung, K.C. Recent advances in peptide macrocyclization strategies. *Chemical Society reviews* **53**, 11725-11771 (2024).